

**BIO-INSPIRED ARTIFICIAL INTELLIGENCE APPROACH
FOR REINFORCED CONCRETE BLOCK SHEAR WALL
SYSTEM RESPONSE PREDICTIONS**

**BIO-INSPIRED ARTIFICIAL INTELLIGENCE APPROACH
FOR REINFORCED CONCRETE BLOCK SHEAR WALL
SYSTEM RESPONSE PREDICTIONS**

By

Hana Elgamel, B.Sc.

A Thesis Submitted to the School of Graduate Studies in Partial Fulfillment of the
Requirements for the Degree of Master of Applied Science

McMaster University

© Copyright by Hana Elgamel, March 2022

Master of Applied Science (2022)
(Civil Engineering)

McMaster University
Hamilton, Ontario

TITLE:

Bio-Inspired Artificial Intelligence
Approach for Reinforced Concrete Block
Shear Wall System Response Predictions

AUTHOR:

Hana Elgamel
B.Sc. (German University in Cairo)

SUPERVISORS:

Dr. Wael El-Dakhkhni

NUMBER OF PAGES:

viii, 56

ABSTRACT

Reinforced concrete block shear walls (RCBSWs) are used as seismic force resisting systems in low- and medium-rise buildings. However, attributed to their nonlinear behavior and composite material nature, accurate prediction of their seismic performance relying only on mechanics is challenging. This study introduces multi-gene genetic programming (MGGP)— a class of bio-inspired artificial intelligence, to uncover the complexity of RCBSW behaviors and develop simplified procedures for predicting the full backbone curve of flexure-dominated fully grouted RCBSWs under cyclic loading. A piecewise linear backbone curve was developed using five secant stiffness expressions associated with cracking, yielding, 80% ultimate, ultimate, and 20% strength degradation (i.e., post-peak stage) derived through controlled MGGP. Based on the experimental results of large-scale cyclically loaded RCBSWs, compiled from previously reported studies, a variable selection procedure was performed to identify the most influential variable subset governing wall behaviors. Utilizing individual wall results, the MGGP stiffness expressions were first trained and tested, and their accuracy was subsequently compared to that of existing models employing various statistical measures. In addition, the predictability of the developed backbone model was assessed at the system-level against experimental results of two two-story buildings available in the literature. The outcomes obtained from this study demonstrate the power of MGGP approach in addressing the complexity of the cyclic behavior of RCBSWs at both component- and system-level—offering an efficient prediction tool that can be adopted by relevant seismic design standards pertaining to RCBSW buildings.

ACKNOWLEDGMENTS

First and foremost, I would like to express my sincere gratitude to my supervisor, Dr. Wael El-Dakhakhni, for his tireless efforts and unparalleled supervision throughout the duration of the research and thesis preparation. Without his insight, encouragement, and availability, I would not have been able to complete this program in the manner and satisfaction that I have. I am also deeply grateful to Dr. Mohamed K. Ismail for his technical support, assistance, and dedicated involvement throughout every step of the process. His valued input and constructive suggestions played an integral part in this research effort. I would like to dedicate this thesis to my parents, Hala and Wael, who taught me the value of hard work by their own example. They have inspired me and pushed me through the toughest of times with their endless support and unconditional love. Finally, all my gratitude goes to my husband and best friend, Ahmed. Without his unwavering support, encouragement, and patience over the last two years, I would not have been able to accomplish what I have.

TABLE OF CONTENTS

Abstract.....	iii
Acknowledgments	iv
1. Introduction	1
2. Research Significance and Methodology	7
3. Model’s Architecture	10
4. Dataset Description	12
5. Data Preprocessing.....	14
5.1 Input Variables Preprocessing.....	15
5.2 Output Variables Preprocessing.....	15
6. Variable Selection.....	17
7. Development of the MGGP Backbone Model	23
7.1 MGGP procedures	23
7.2 MGGP Parameters.....	28
8. Final MGGP-based Expressions	30
9. Component-Level Model Performance Assessment	33
10. System-Level Model Performance Assessment	38
11. Sensitivity Analyses	43
12. Conclusions	46
13. References	49

LIST OF TABLES

Table 1. Potential candidate input variables and outputs used in the development of the backbone model	16
Table 2. Main parameters of the developed MGGP-based expressions	29

LIST OF FIGURES

Figure 1. Proposed backbone models for RCBSWs by (a) Ashour and El-Dakhakhni [10], (b) Ashour and Galal [11], and (c) Ezzeldin et al. [12]	5
Figure 2. Study organization and methodology	9
Figure 3. Proposed Backbone model	12
Figure 4. Distribution of the RCBSWs design parameters	14
Figure 5 Selection procedure for subsets of potential input variables for (a) <i>KcrKg</i> , (b) <i>KyKg</i> , (c) <i>K0.8u'Kg</i> , (d) <i>KuKg</i> , and (e) <i>K0.8uKg</i>	19
Figure 6. Variable selection procedure for combinations of potential input variables for (a) <i>KcrKg</i> , (b) <i>KyKg</i> , (c) <i>K0.8u'Kg</i> , (d) <i>KuKg</i> , and (e) <i>K0.8uKg</i>	21
Figure 7. Correlation matrix for the selected variables when y equals to: a) <i>KcrKg</i> , b) <i>KyKg</i> , c) <i>K0.8u'Kg</i> , d) <i>KuKg</i> , and e) <i>K0.8uKg</i>	22
Figure 8. An example of MGGP process	25
Figure 9. Flowchart representation of MGGP procedure	27
Figure 10. Procedures to generate the proposed backbone model	32
Figure 11. Predictability of the MGGP model compared to other existing models	34
Figure 12. Statistical indicators of displacement predictions at (a) yielding, (b) ultimate, and (c) 20% strength degradation	37

Figure 13. The predicted backbone curves of individual RCBSWs in Buildings II tested by Heerema et al. [47] and III tested by Ashour and El-Dakhakhni [10]...	41
Figure 14. Superimposition of RCBSW components backbone model generated using MGGP model compared to experimental backbone model obtained from (a) Building II tested by Heerema et al. [47], and (b) Building III tested by Ashour and El-Dakhakhni [10].....	43
Figure 15. Effect of parameters on the performance stiffness expressions, where V refers to any independent variable from Eqs. 7a-7e	45
Figure 16. Sensitivity analysis of input design parameters in developed MGGP-based expressions.....	46

1. INTRODUCTION

Considering the proliferation of low- and mid-rise buildings, the use of reinforced concrete block shear walls (RCBSWs) as a seismic force-resisting system has been receiving great attention. In the past, RCBSW buildings were constructed without adequate reinforcement detailing accounting for seismic demands [1-2]. For example, field surveys in the aftermath of severe earthquakes such as the 2010 Maule and the 2014 Iquique earthquakes, demonstrated that a significant number of RCBSWs were severely damaged and even completely collapsed [2-4]. Subsequently, new design and prescriptive detailing requirements have been introduced by relevant design standards (e.g., ASCE/SEI 41-17 [5], CSA S304-14 [6], and TMS 402-11 [7]) to realize improved RCBSWs seismic performance. In parallel, extensive research studies have been performed to evaluate the seismic response of RCBSWs, which was found to be highly influenced by their shear-span ratios, the magnitude of the applied axial loads, and the horizontal and vertical reinforcements [8-9]. However, the complexity of RCBSWs as a composite structural component (i.e., made up of different interacting nonlinear materials) remains a challenge for accurate prediction of wall behavior under seismic loading. A few researchers attempted to address this issue by modeling the load-displacement backbone curve of RCBSWs under cyclic loading through analytical and empirical approaches.

Ashour and El-Dakhakhni [10] proposed a trilinear backbone curve for fully grouted RCBSWs using three secant stiffness expressions (Eqs. 1a-1c) for yielding (K_y), ultimate (K_u), and 20% strength degradation ($K_{0.8u}$) (as shown in **Fig. 1a**). The backbone curve was developed based on the experimental results of four individual RCBSWs tested under lateral cyclic loads.

$$K_y = 1 / \left(\frac{h_w^3}{3E_m I_e} + \frac{1.2h_w}{G_m A_e} \right), \quad K_u = 0.6 \times K_y, \quad K_{0.8u} = 0.2 \times K_y \quad (1a)$$

$$G_m = 0.4 E_m, \quad I_e = \alpha I_g, \quad A_e = \alpha A_g, \quad \alpha = \left(\frac{100}{f_y} + \frac{P_u}{f'_m A_g} \right) \quad (1b)$$

$$\Delta_y = \frac{Q_y}{K_y}, \quad \Delta_u = \frac{Q_u}{K_u}, \quad \Delta_{0.8u} = \frac{Q_{0.8u}}{K_{0.8u}} \quad (1c)$$

where h_w is the wall height, I_g is the wall gross moment of inertia, I_e is the wall effective moment of inertia, A_e is the wall effective area, A_g is the wall gross area, E_m is the masonry elastic modulus, G_m is the masonry shear modulus, f'_m is the masonry compressive strength, f_y is the reinforcement yielding strength, Δ_y , Δ_u , and $\Delta_{0.8u}$ are the displacements corresponding to yielding strength (Q_y), ultimate strength (Q_u), and 20% strength degradation ($Q_{0.8u}$), respectively.

Ashour and Galal in 2017 [11], proposed a modification to K_y , K_u , and $K_{0.8u}$ (presented in Eqs. 2a-2b) originally developed by Ashour and El-Dakhakhni [10]. In addition, a new secant stiffness expression was introduced to the backbone curve defining the stiffness up to cracking (K_{cr}). **Figure 1b** shows the

quad-linear modified backbone curve that was developed by Ashour and Galal in 2017 [11] based on a dataset consisted of 25 RCBSWs.

$$K_{cr} = K_g = 1 / \left(\frac{h_w^3}{3E_m I_g} + \frac{1.2h_w}{G_m A_g} \right), K_P = \alpha K_g \quad (2a)$$

$$K_y = -0.00096 K_P^2 + 0.89801 K_P, K_u = 0.2875 \times K_y, K_{0.8u} = 0.5479 \times K_u \quad (2b)$$

Ezzeldin et al. [12] also proposed a trilinear moment-rotation backbone model for RCBSWs (**Fig. 1c**) based on the ASCE/SEI 41-17 [5] originally proposed for reinforced concrete shear walls. The proposed model was validated at the system level against the results of eight RCBSWs with and without boundary elements. As shown in **Fig. 1c**, Ezzeldin et al. [12] model defined the elastic zone up to point *B* by the elastic rotation (θ_y), whereas parameter *a* and *b* were used to represent the plastic rotation up to the ultimate strength (θ_u) and failure (θ_r) at point *C* and *E*, respectively. The parameter *c* is also suggested to quantify the residual moment (M_r) at point *D*. In their study [12], Ezzeldin et al. evaluated the yielding, ultimate, and residual strengths (Q_y , Q_u , and Q_r , respectively) by dividing the corresponding moments by the wall heights, whereas the displacements at yield, ultimate, and residual strengths (Δ_y , Δ_u and Δ_r , respectively) are calculated according to Eqs. 3a-3c.

$$\Delta_y = \frac{Q_y}{K_y}, K_y = \alpha K_g \quad (3a)$$

$$\Delta_{max} = \Delta_y + a(h - l_p) \quad (3b)$$

$$\Delta_r = \Delta_y + b(h - l_p) \quad (3c)$$

where, $a = 0.006$ rad, $b = 0.015$ rad, $c = 60\%$, and l_p is the plastic hinge length of the wall that was assumed to be 50% of the wall flexural depth but less than the wall height and less than 50% of the wall length, according to ASCE/SEI 41-17 [5].

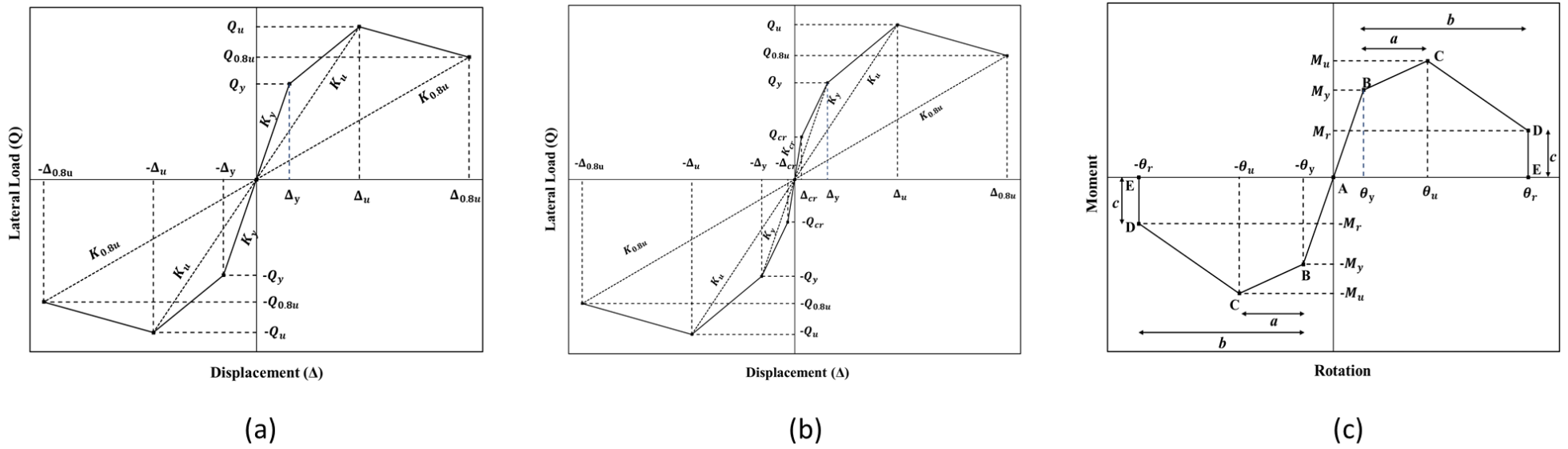


Figure 1. Proposed backbone models for RCBSWs by (a) Ashour and El-Dakhakhni [10], (b) Ashour and Galal [11], and (c) Ezzeldin et al. [12]

The predictability of the available backbone models can be restricted by the fact that a limited number of RCBSW test results were used in their development and validation (i.e., a maximum of 25 walls). In addition, these models were produced employing basic mechanics, simplified regression analyses, and without performing variables selection procedures to determine the key parameters controlling the seismic performance of RCBSWs. As such, the methodologies adopted for the development of current models may not be able to accurately uncover the non-linear interactions between the influencing (input) parameters and their relationships with the resulting wall behavior (output). Available models were also not assessed using new datasets, not used in their development—posing challenges to model generalizability. Subsequently, developing more efficient procedures to accurately predict the response of RCBSWs remains essential for efficient seismic design.

Recently, several studies employed artificial techniques (AI) to interpret complex, multivariant behaviors in structural engineering (such as predicting the lateral drifts of reinforced masonry shear walls [13]) due to their ability to capture nonlinear input-output relationships. Genetic programming (GP) is one of the AI techniques that follows Darwinian principles [14] to find the near-optimal mathematical model relating the system input variables to the sought-after target (output) [15-16]. In recent studies, GP and its more powerful variant (i.e., multi-gene genetic programming (MGGP)) have been utilized to predict the creep of

concrete [17], the shear strength of short rectangular reinforced concrete columns [18], the compressive strength of geopolymer concrete [19], the bond strength of composite bars in concrete [20], the degree of steel corrosion damage in reinforced concrete [21], the shear-strength of squat reinforced concrete walls with boundary elements [22], the shear strength of steel fibers reinforced concrete beams [23-24].

The capabilities of MGGP were thus utilized in this study to develop the necessary expressions to generate the backbone curve of fully grouted RCBSWs. A variable selection procedure was performed to identify the key parameters affecting the seismic response of RCBSWs. The MGGP-based model was developed, trained, and tested using the results of 74 RCBSWs compiled from literature. The prediction performance of the developed MGGP-based backbone model was assessed at the component- and system-levels and was also compared against existing available models. Finally, sensitivity analyses were conducted to provide further insights into the extents of the influences of each input parameter on the prediction performance of the developed MGGP model.

2. RESEARCH SIGNIFICANCE AND METHODOLOGY

Achieving accurate load-displacement backbone curve for cyclically loaded RCBSWs is key to define various response characteristics such as initial stiffness, cracking, yielding and ultimate strengths, ductility, energy dissipation

capacity, and post-peak behavior. The MGGP approach was employed herein to capture the complex nonlinearity controlling the relationships between the different design parameters and the walls' response. The developed MGGP-based backbone curve model empowers practicing engineers and designers with an essential tool to quantify RCBSW building response and subsequently pertinent seismic risk.

For this purpose, the current study starts by briefly describing the proposed MGGP backbone model architecture and experimental dataset. Subsequently, a variable selection procedure was performed to identify the most influential parameters among a list of potential candidates selected based on previous research findings and existing models. Using the considered dataset, the MGGP searched for the best fit expression considering the selected influential parameters for each specified point (i.e., cracking, yielding, 80% of the ultimate strength, ultimate strength, 20% strength degradation). After that, the MGGP-based backbone model was assessed against existing models available in the literature using various statistical measures. The predictability of the developed model was also evaluated at the system-level using further available experimental results. Finally, sensitivity analyses were performed to evaluate the influences of each parameter on the prediction performance of the developed expressions. **Figure 2** displays the organization and methodology of the current study.

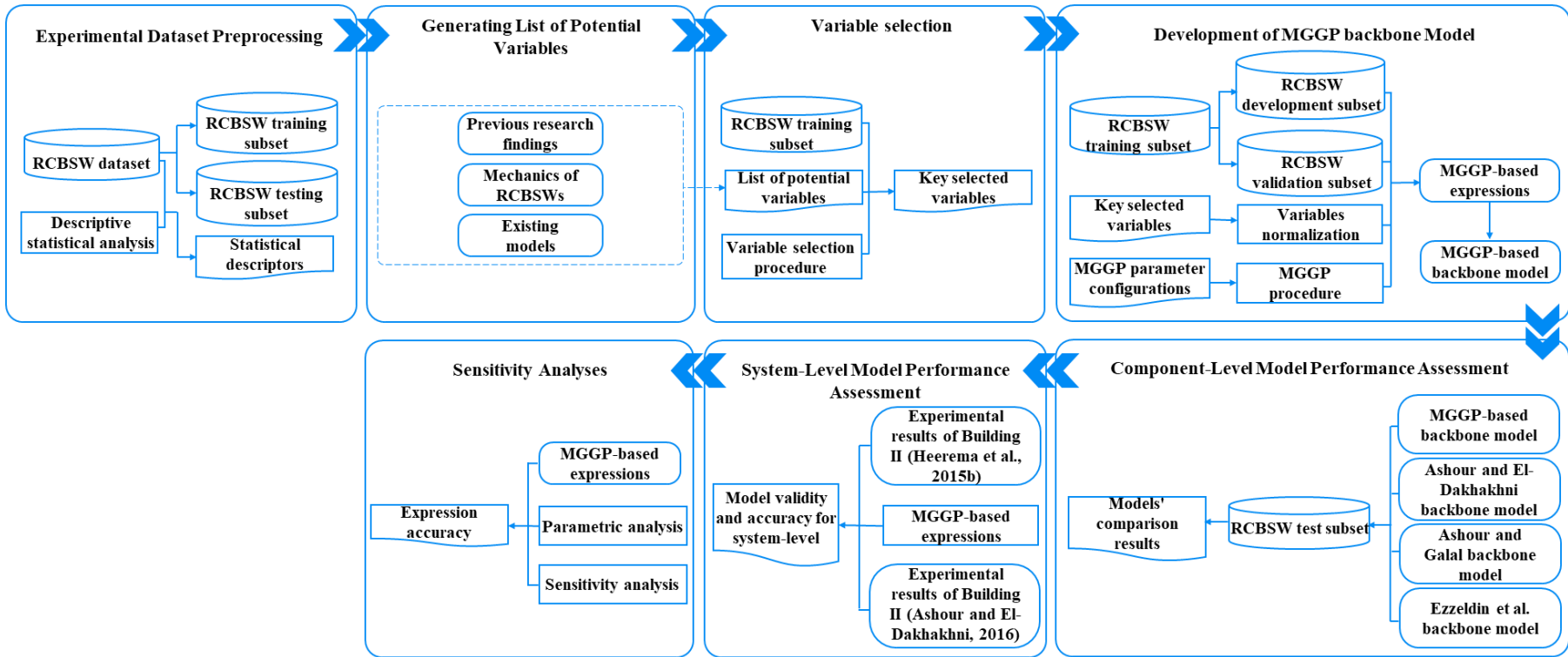


Figure 2. Study organization and methodology

3. MODEL'S ARCHITECTURE

Figure 3 shows the proposed load-displacement backbone model, which was defined by five key points, as follows:

- The first point refers to the cracking initiation. The cracking load (Q_{cr}) is computed by enforcing equilibrium, assuming a fixed masonry flexure tensile strength of 0.65 MPa, as recommended by the CSA [6].
- The second point refers to the initiation of yielding in the outermost reinforcement bar. The corresponding yielding load (Q_y) is calculated using mechanics principles (i.e., force equilibrium and strain compatibility conditions).
- By examining the backbone curves of the tested RCBSWs included in the dataset, no significant reduction in the wall stiffness was observed corresponding to the second point, although the outermost reinforcement bar reached its yielding stress. The curves descend at an average load value of 80% of the ultimate load ($Q'_{0.8u}$) [25-26]. Therefore, the point corresponding to 80% of the ultimate load was defined as the third point on the proposed backbone model to represent the yielding of the wall element. The value of $Q'_{0.8u}$ is simply calculated by multiplying the ultimate load by 0.8.

- The fourth point refers to ultimate strength of RCBSWs. At this point, the ultimate load (Q_u) is calculated using force equilibrium and strain compatibility, assuming masonry reached its ultimate compression strain of 0.0025.
- The fifth point refers to a 20% degradation in the strength ($Q_{0.8u} = 0.8 * Q_u$).
- The Δ_{cr} , Δ_y , $\Delta'_{0.8u}$, Δ_u , and $\Delta_{0.8u}$ are the displacement values corresponding to the loads Q_{cr} , Q_y , $Q'_{0.8u}$, Q_u , and $Q_{0.8u}$, respectively.
- Then, the stiffnesses of the five key points (K_{cr} , K_y , $K'_{0.8u}$, K_u , and $K_{0.8u}$) can be expressed as shown in Eq. 4 next:

$$K_{cr} = Q_{cr} / \Delta_{cr}, K_y = Q_y / \Delta_y, K'_{0.8u} = Q'_{0.8u} / \Delta'_{0.8u}, K_u = Q_u / \Delta_u, K_{0.8u} = Q_{0.8u} / \Delta_{0.8u}$$

(4)

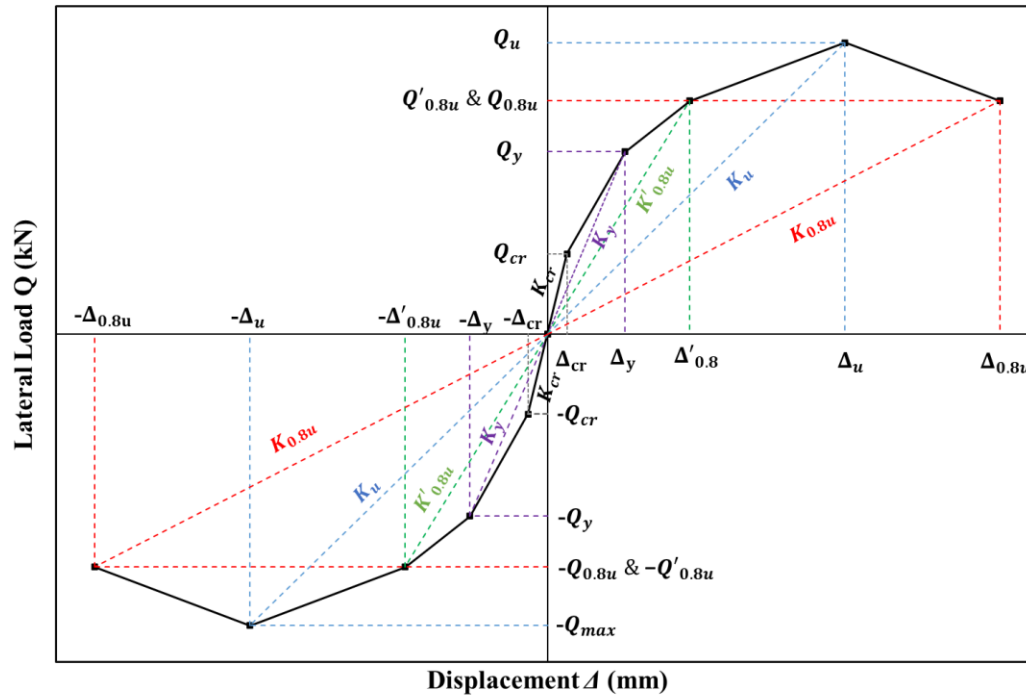


Figure 3. Proposed Backbone model

4. DATASET DESCRIPTION

The dataset utilized in the current study includes the design parameters and experimental backbone curves of 74 cyclically loaded RCBSWs collected from previous studies including: Eikanas (6 walls) [26], Priestley & Elder (2 walls) [27], Shing (11 walls) [28], Shedid et al. (6 walls) [29], Shedid et al. (2 walls) [30], Sherman (8 walls) [31], Hernandez (3 walls) [32], Siam et al. (4 walls) [33], Kapoi (8 walls) [34], and Ahmadi et al. (24 walls) [35]. It is worth noting that all walls considered within the dataset were: *i*) fully grouted, *ii*)

vertically and transversally reinforced, *iii*) tested under displacement controlled, in-plane quasi-static, reversed cyclic lateral loading, and *iv*) failed in flexure.

The design parameters included in the collected dataset are: wall length (l_w), wall thickness (t_w), wall height (h_w), horizontal reinforcement ratio (ρ_h), vertical reinforcement ratio (ρ_v), yield and ultimate strength of vertical reinforcement steel bars (f_{yv}, f_{uv} , respectively), yield and ultimate strength of horizontal reinforcement steel bars (f_{yh}, f_{uh} , respectively), compressive strength of grouted masonry units (f'_m), and the axial compressive load (P). The distribution of the wall design parameters is illustrated in **Fig. 4**. The figure shows the minimum, first quartile, median, third quartile, and maximum values of each design parameter. As an example, the wall height (h_w) had a minimum, first quartile, median, third quartile, and maximum values of 1321 mm, 1830 mm, 2032 mm, 2845 mm, and 3990, respectively.

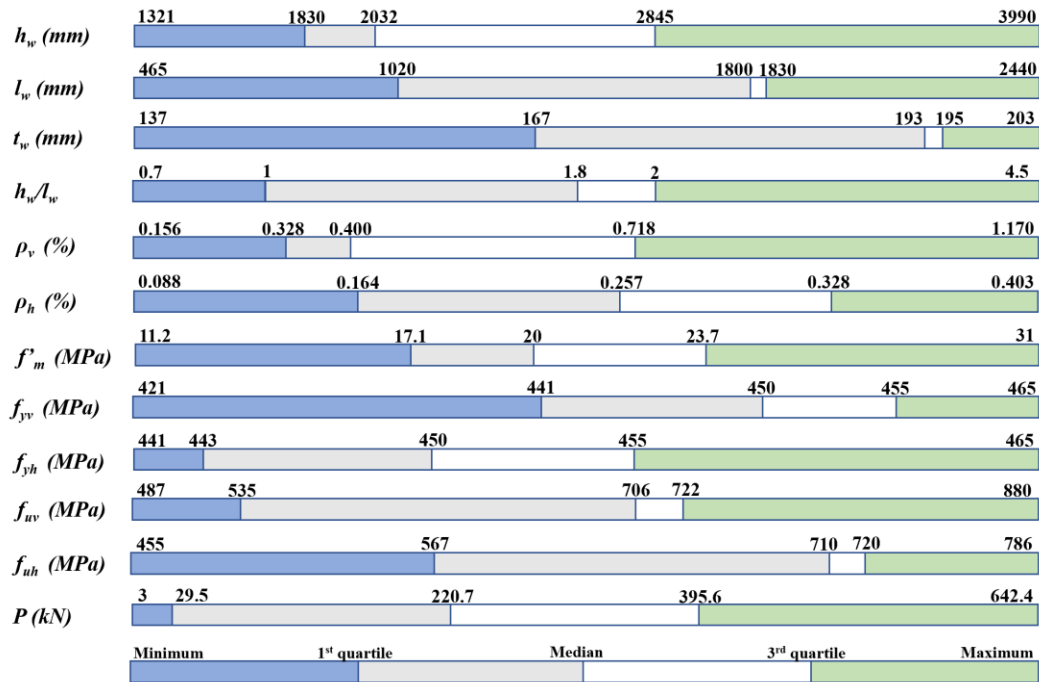


Figure 4. Distribution of the RCBSWs design parameters

5. DATA PREPROCESSING

Although the power of MGGP stems from its capacity to consider a very large number (search space) of possible combinations of system variables and mathematical relationships, MGGP does not specifically consider the variable units or dimensions. Therefore, a key data pre-processing step was performed to ensure that the parameters extracted from the experimental dataset are presented to the MGGP algorithm in a way that facilitate mechanics-supported understanding of the relationships between the input and output variables.

5.1 Input Variables Preprocessing

Wall design parameters (i.e., input parameters) have different units; for example, wall's length l_w has a unit of length, yield strength of reinforcement steel bars f_{yv} has a unit of stress, and axial compressive load P has a unit of force. To avoid generating dimensionally inconsistent prediction expressions, all input variables were normalized, forming dimensionless candidates, in order to control the shape/combination of the variables included in the MGGP resulting expressions. The design parameters were presented through six dimensionless candidates, namely the wall aspect ratio (h_w/l_w), axial load ratio ($P/A_w \cdot f'_m$), vertical reinforcement ratio (ρ_v %), horizontal reinforcement ratio (ρ_h %), $\rho_v \cdot f_y / f'_m$, $\rho_h \cdot f_y / f'_m$. These candidates were chosen based on previous research findings and engineering understanding for the mechanics of RCBSWs.

5.2 Output Variables Preprocessing

The output variables were the stiffness of the specified five key points: K_{cr} , K_y , $K'_{0.8u}$, K_u , and $K_{0.8}$, which were first calculated according to Eq. 4 by dividing the load at each point (analytically obtained from mechanics principles) by the corresponding displacement (graphically obtained from the experimental backbone curves of the tested RCBSWs). Then, the K_{cr} , K_y , $K'_{0.8u}$, K_u , and $K_{0.8}$ values were normalized by the theoretical gross stiffness of RCBSWs, $K_g =$

$1/\left(\frac{h_w^3}{3E_m l_g} + \frac{1.2h_w}{G_m A_g}\right)$ that was proposed by Paulay and Priestley [25], where $E_m = 900 f'_m$ and $G_m = 0.4 E_m$. **Table 1** shows the list of potential inputs and output variables.

Table 1. Potential candidate input variables and outputs used in the development of the backbone model

Input variable ID	Physical formulation
x_1	h_w/l_w
x_2	$P/A_w \cdot f'_m$
x_3	$\rho_h \%$
x_4	$\rho_v \%$
x_5	$\rho_v \cdot f_y / f'_m$
x_6	$\rho_h \cdot f_y / f'_m$
Output variable ID	Physical formulation
y_1	K_{cr}/K_g
y_2	K_y/K_g
y_3	$K'_{0.8u}/K_g$
y_4	K_u/K_g
y_5	$K_{0.8u}/K_g$

6. VARIABLE SELECTION

The inclusion of too many or too few input variables in the modeling usually leads to unnecessarily complexity or inaccurate prediction expressions. As such, the identification of the most relevant input variables is key to achieve efficient and elegant expressions for practicing engineers. Subsequently, in this study, the best subset selection procedure (*BSS*) was adopted to select the most influential subset of independent variables on the cyclic behavior of RCBSWs.

For k independent variables, the *BSS* procedure begins by considering all possible expressions with size 1, size 2, ..., size k (i.e., consist of 1 variable, 2 variables, ..., k variables, respectively). Subsequently, the best expression for each size is identified, and, eventually, the best overall expression was selected from these finalists. This procedure is known to be computationally demanding unlike the forward and backward stepwise procedures which are more efficient [36]; however; the *BSS* was selected in the current study since the number of independent variables is not very large. The method used to evaluate the performance of the expressions generated at each step of the *BSS* technique is also important [36]. The use of R^2 and *RMSE* measures, for example, are insufficient for assessing the performance of various expressions with different number of variables. This is attributed to the fact that, when additional variables are added to the expression in each step, the former increases (i.e., R^2) while the latter decreases (i.e., *RMSE*), resulting in a highly complex expression. Due to the

biased nature of such measures—based only on the training set performance, expression's poor testing set performance is not unexpected [36].

Based on the above-mentioned factors, the Bayesian information criterion (*BIC*) was selected as the expression performance evaluation measure. The *BIC* value for a prediction expression is computed as in Eq. 5:

$$BIC = \frac{1}{n\sigma^2} (\sum_{i=1}^n (y_i - y_i^*)^2 + \log(n)d\sigma^2) \quad (5)$$

where σ^2 is the variance of residual errors between expression predictions and experimental observations; n is the number of observations; $\sum_{i=1}^n (y_i - y_i^*)^2$ is the total sum of squares; and d is the number of variables included within the expression in a certain step [36-38]. The *BIC* applies a penalty on the *RMSE* that is only computed considering the expression performance on the training set. Hence, the penalty incorporates any bias in the training set due to overfitting, and in turn, implicitly accounts for the fact that the expression's performance on the training set is not representative of its performance on the testing set [37-38]—improving expression generalizability. Furthermore, *BIC* penalizes unnecessarily complexity by increasing penalties for expressions with more variables through the factor $(\log(n)d\sigma^2)$ presented in Eq. 5. [36]. This penalty explains the possibility of multicollinearity of variables and prevents the inclusion of two variables that represent the contribution of the same wall's design characteristic. Finally, and similar to *RMSE*, lower *BIC* values are an indication of better expression predictions.

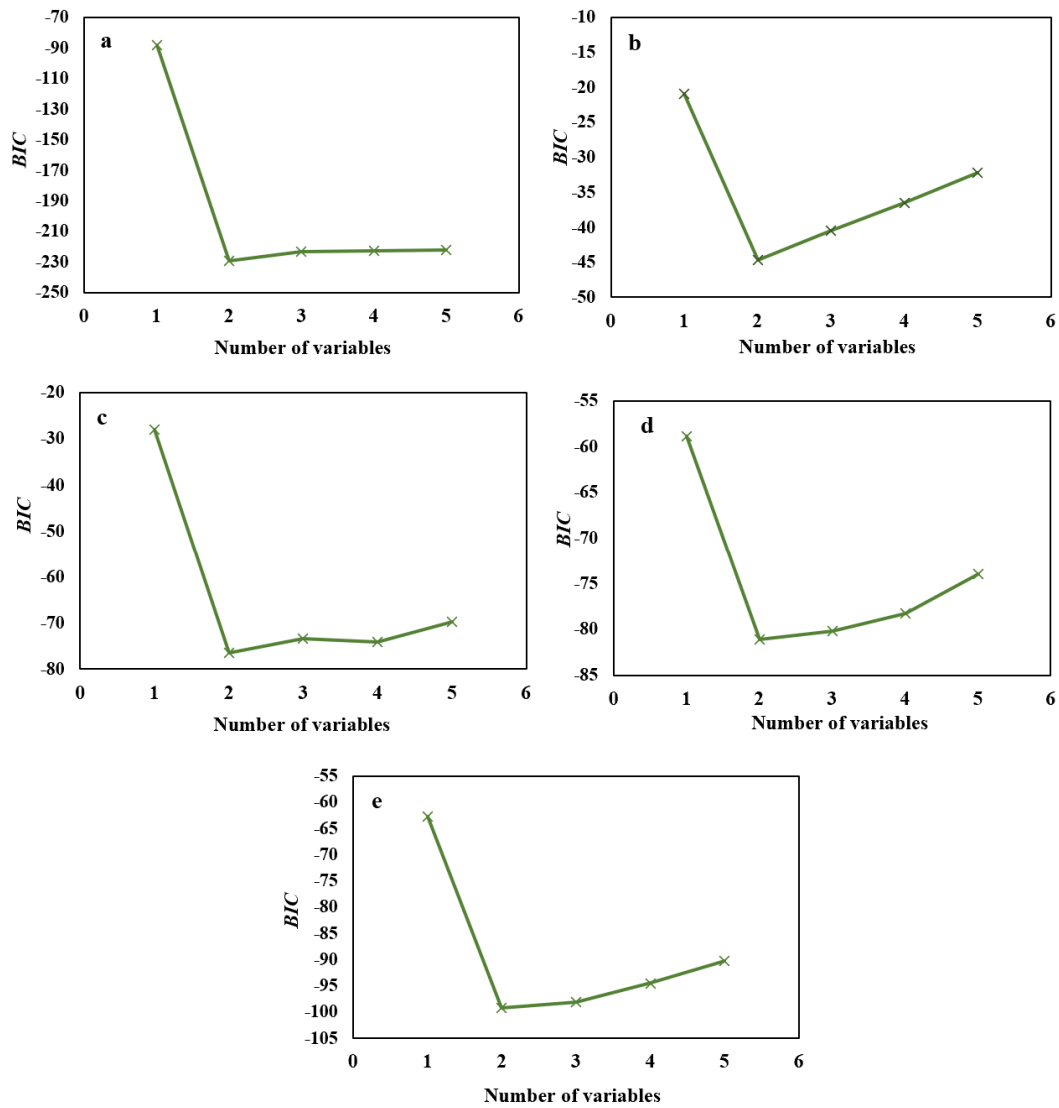


Figure 5 Selection procedure for subsets of potential input variables for (a)

$$\frac{K_{cr}}{K_g}, \text{ (b) } \frac{K_y}{K_g}, \text{ (c) } \frac{K'_{0.8u}}{K_g}, \text{ (d) } \frac{K_u}{K_g}, \text{ and (e) } \frac{K_{0.8u}}{K_g}$$

Prior to performing the *BSS* procedure, the variable $x_1 = \frac{h_w}{l_w}$ was removed to eliminate any complexity or duplications, since the equation of K_g (which was used in normalizing the output variables) considers the influence of

h_w/l_w . Subsequently, the *BSS* procedures were performed on only five input parameters (x_2, x_3, x_4, x_5 , and x_6) (listed in **Table 1**) against each output variable ($\frac{K_{cr}}{K_g}, \frac{K_y}{K_g}, \frac{K'_{0.8u}}{K_g}, \frac{K_u}{K_g}, \frac{K_{0.8u}}{K_g}$). **Figure 5** indicates that the best subset includes two variables since this number of variables provides the lowest *BIC* value out of all possible subsets. The inclusion of additional variables provides no further enhancement to the expression performance. **Figure 6** also demonstrates that the best subset (i.e., corresponding to the darkest shade) is a combination of the variables x_2 and x_4 ($P/A_w \cdot f'_m$ and ρ_v , respectively), ranked according to their influence on each stiffness ratio. Therefore, these two variables were only utilized to develop the MGGP-based expressions.

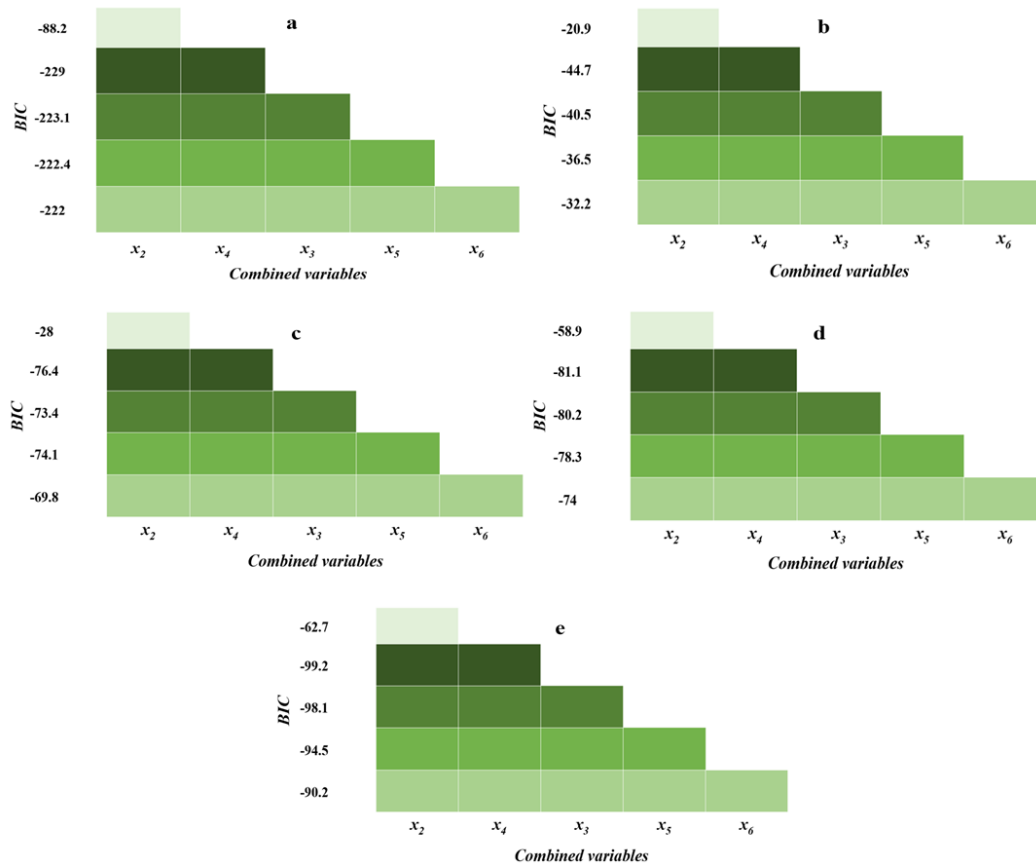


Figure 6. Variable selection procedure for combinations of potential input

variables for (a) $\frac{K_{cr}}{K_g}$, (b) $\frac{K_y}{K_g}$, (c) $\frac{K'_{0.8u}}{K_g}$, (d) $\frac{K_u}{K_g}$, and (e) $\frac{K_{0.8u}}{K_g}$

Figure 7 shows the correlation matrices between the input variables (x_2 and x_4) and each stiffness ratio (output variable). The diagonal boxes in the figures display the distribution of each variable, the boxes in the upper-right region demonstrate the Pearson product correlation coefficient (R) that quantifies the strength of the relationship between every pair of variables, and the boxes in the lower-left region present the fitted lines of the scatter plots between every pair of variables. As can be seen, each stiffness ratio appeared to have a positive direct

relationship in general with both variables (x_2 and x_4).

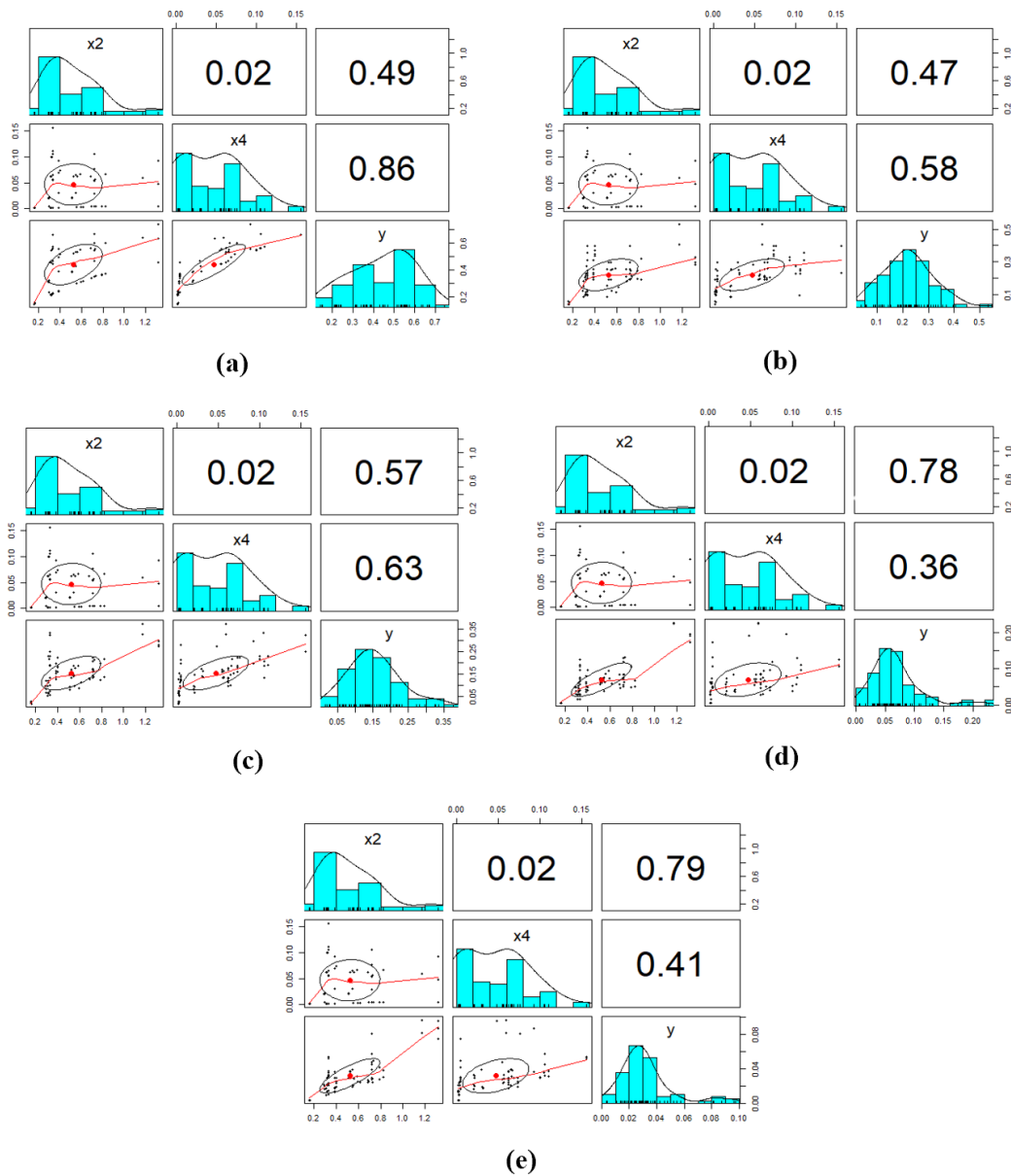


Figure 7. Correlation matrix for the selected variables when y equals to: a)

$$\frac{K_{cr}}{K_g}, \text{ b) } \frac{K_y}{K_g}, \text{ c) } \frac{K'_{0.8u}}{K_g}, \text{ d) } \frac{K_u}{K_g}, \text{ and e) } \frac{K_{0.8u}}{K_g}$$

7. DEVELOPMENT OF THE MGGP BACKBONE MODEL

In order to form the backbone model, the MGGP, through the MATLAB© toolbox GPTIPS [39], was employed to develop the early identified five secant stiffness expressions, in a form of $\frac{K_i}{K_g} = f\left(\frac{P}{A_w \cdot f'_m}, \rho_v\right)$, where K_i refers to the K_{cr} , K_y , $K'_{0.8u}$, K_u , and $K_{0.8u}$.

The dataset was divided into a training subset (70% of the total data set) and a testing subset (30% of the total data set) in a stratified manner, where both sets have similar statistical properties, as recommended by Ahangar-Asr et al. [40]. The training subset is first used to develop and validate the MGGP-based stiffness expressions, and the testing subset is successively used to evaluate the predictability of the developed expressions for unseen dataset that has not been use in their development.

7.1 MGGP procedures

The GP algorithm is based on the Darwinian theory of “Survival of the fittest”, it finds the optimal solution by simulating the process of evolution in nature on populations of hundreds or thousands of computer programs. In other words, GP can reach the near-optimal solution for complex systems by extensively searching for the best fit expression between all potential expressions [41]. GP evolves a population of trees through implementing symbolic regression,

where the evolved expressions predict output vectors (y) equal to the number of observations of the response variables using corresponding matrix of inputs (x) equal to the number of observations of the response variables multiplied by the number of input variables. Building on GP, in MGGP each symbolic model, or each member of the GP population, is a weighted linear combination of the outputs from several GP trees “genes” [42].

The MGGP procedure starts with the user specifying several preparatory selections such as: 1) the terminal set; 2) the set of primitive functions; 3) the fitness measure; 4) certain parameters for controlling the run; and 5) the termination criterion and method for designating the result of the run [43]. Users specify the maximum allowable number of genes, G_{\max} , and the maximum tree depth for a model, therefore—controlling the model complexity. Furthermore, to attain a relatively compact model, the maximum tree depth could be restricted to 4 or 5 nodes for instance [42].

The set of primitive functions could be basic mathematics operations (+, -, \times , /, etc.), non-linear functions (sin, cos, tan, exp, tanh, log), Boolean logic functions (AND, OR, NOT, etc.), or any other mathematical functions; while the terminal set comprises the arguments for these functions and could consist of numerical constants, logical constants, variables etc. [44]. The fourth selection entails the control parameters specification such as the population size, and the fifth selection includes the specification of the maximum number of generations

to be run [44]. After completing the five selections steps, the MGGP run can be launched. The procedure of a MGGP run could be summarized in four major steps as presented by [42].

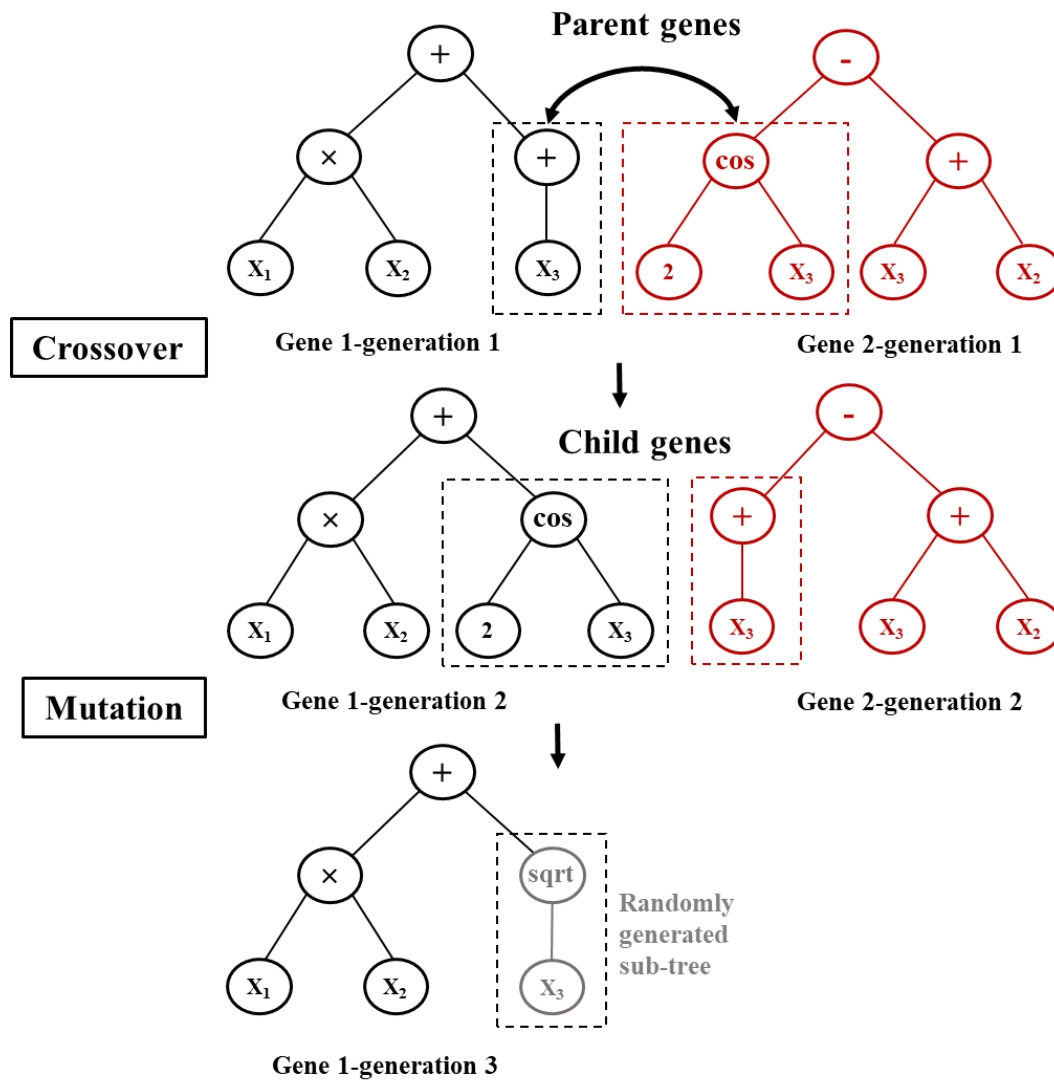


Figure 8. An example of MGGP process

First, the initial population is formed by randomly creating individuals containing GP trees with different genes (between 1 and G_{\max}), each individual represents a potential expression for predicting the RCBSW stiffness. Second, a fitness value is assigned to each individual indicating its accuracy to predict the output. Third, based on this fitness value, genetic operations (elitism, crossover, mutation) are performed on the models to evolve a new population. Individuals with high fitness values are directly reproduced to a new population (elitism), while mutation and crossover operations are performed on the remaining individuals. Two-point high-level crossover is performed in addition to the traditional crossover as it allows the exchange of genes between individuals and even the removal of genes. The mutation operation is replacing a branch of the model with another randomly generated model. An example of a typical evolutionary process for an MGGP model is presented in **Fig. 8**. Fourth, the genetic operations are continuously performed on the populations' individuals as long as the termination criterion is not met, and once it is met, the model is finally selected based on the minimum fitness value and its performance is assessed on testing data [41]. **Figure 9** shows the MGGP modeling procedures.

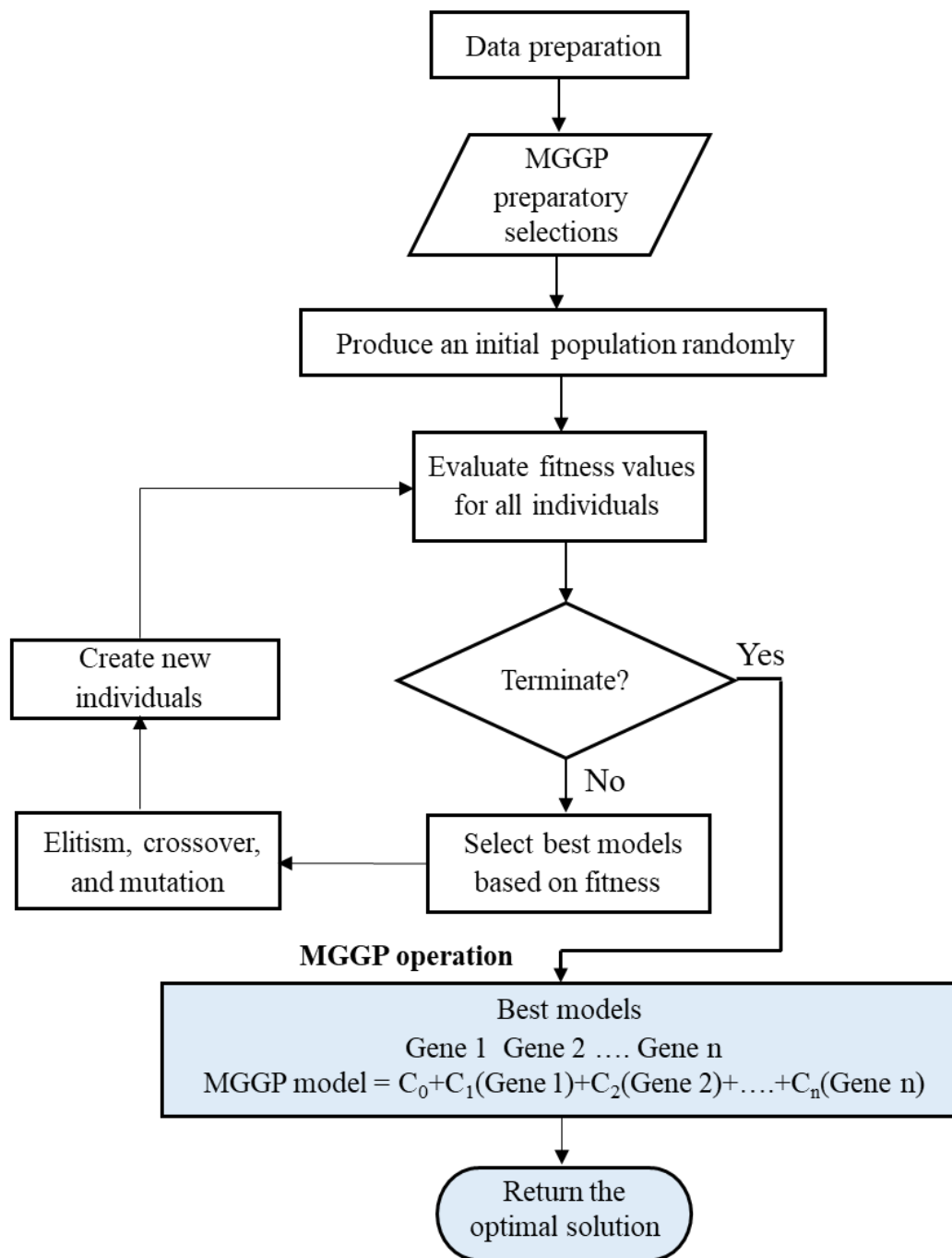


Figure 9. Flowchart representation of MGPP procedure

7.2 MGGP Parameters

In this study, several combinations of MGGP parameter configurations were selected to perform multiple runs. Subsequently, the performance of developed expressions in each run was evaluated based on their accuracy and simplicity, until the near-optimal MGGP-based expressions were chosen. **Table 2** presents the final MGGP parameters used to develop the best performing expressions. A population size of 1000 individuals was selected to provide a wide enough search space for the MGGP procedure. The number of generations was set to 1000 as it led to the best fitness values on both training and testing subsets, and also the termination criterion was set to reach either this number of generations or fitness function equal to 1. The maximum number of genes and tree depth were set to a value of 2 and 3, respectively, to achieve accurate yet simple enough expressions. In addition, only the basic functional relationships of addition, subtraction, multiplication, and power were used. The probability rates of crossover, mutation, and elitism were set at 85%, 10%, and 5%, respectively, for maximum model efficiency [45-46].

Table 2. Main parameters of the developed MGGP-based expressions

Parameter	Setting
Population size (P)	1000
Number of generations (N)	1000
Termination criterion	Number of generations
Fitness function	$\frac{1}{R^2} + NRMSE$
Number of genes	2
Maximum tree depth	3
Function set	(+), (-), (\times), and power
Elitism fraction	0.05
Individual selection method for crossover and mutation	Tournament selection
Tournament size	2
Crossover rate	0.80
Mutation rate	0.15

The MGGP expression accuracies were evaluated using the fitness function which combines both the squared correlation coefficient (R^2) and the normalized root-mean-square error ($NRMSE$) (Eq. 6a-c). This fitness function qualifies the evaluation of both the linear correlation and the aggregated residual error between the MGGP-based predictions and experimental observations. The optimum value of the *fitness function* is equal to 1.0 (ideally when $R^2 = 1$ and $NRMSE = 0$), as such, the higher the R^2 and the lower the $NRMSE$ values, the more the expression is accurate.

$$R^2 = \left(\frac{\sum_{i=1}^n (y_i - \bar{y})(y_i^* - \bar{y}^*)}{\sqrt{\sum_{i=1}^n (y_i - \bar{y})^2 (y_i^* - \bar{y}^*)^2}} \right)^2 \quad (6a)$$

$$NRMSE = \frac{\sqrt{\frac{1}{n} \sum_{i=1}^n (y_i - y_i^*)^2}}{\bar{y}_i} \quad (6b)$$

$$Fitness = \frac{1}{R^2} + NRMSE \quad (6c)$$

8. FINAL MGGP-BASED EXPRESSIONS

The final MGGP-generated expressions are summarized in Eqs. 7a-7e:

$$K_{cr} = \left[2 \left(\frac{P}{f_{mAg}} \right) + 1.18 \rho_v^{0.2} - 0.71 \right] K_g \quad (7a)$$

$$K_y = \left[1.1 \left(\frac{P}{f_{mAg}} \right)^{0.85} + 0.75 \rho_v^{0.15} - 0.53 \right] K_g \quad (7b)$$

$$K'_{0.8u} = \left[7.64 \left(\frac{P}{f_{mAg}} \right)^{1.78} + 0.5 \rho_v^{0.2} - 0.32 \right] K_g; \text{ where } K'_{0.8u} \leq 0.7K_y \quad (7c)$$

$$K_u = \left[0.13 \left(\frac{P}{f_{mAg}} \right)^{0.55} + 0.1 \rho_v^{1.25} \right] K_g \quad (7d)$$

$$K_{0.8u} = \left[0.16 \left(\frac{P}{f_{mAg}} \right) + 0.05 \rho_v^{1.2} \right] K_g; \text{ where } K_{0.8u} \leq 0.5K_u \quad (7e)$$

It should be noted that in Eq. 7c, the stiffness values corresponding to the yielding of wall element should not exceed 0.7 of the stiffness values corresponding to the yielding of the outermost reinforcement bar. Also, in Eq. 7e, the stiffness values corresponding to 20% strength degradation should not exceed

0.5 of the stiffness values corresponding to the ultimate strength.

Using the developed expressions, the five specified stiffnesses can be calculated. Subsequently, by enforcing equilibrium and compatibility strain conditions, the crack, yield, and ultimate strengths can be obtained. The ultimate strength is multiplied by 0.8 to be reduced by 20% in order to obtain $Q'_{0.8u}$ and $Q_{0.8u}$. Then, the five strength values are divided by the five stiffness values to obtain the five corresponding displacement values. Finally, using the strengths and corresponding displacements, the penta-linear backbone curve can be plotted. Although the developed expressions are generalizable to other RCBSWs not used in training, they may only be valid for walls with design parameters that fall within the examined ranges. The flowchart in **Fig. 10** summarizes the procedures of generating the backbone model.

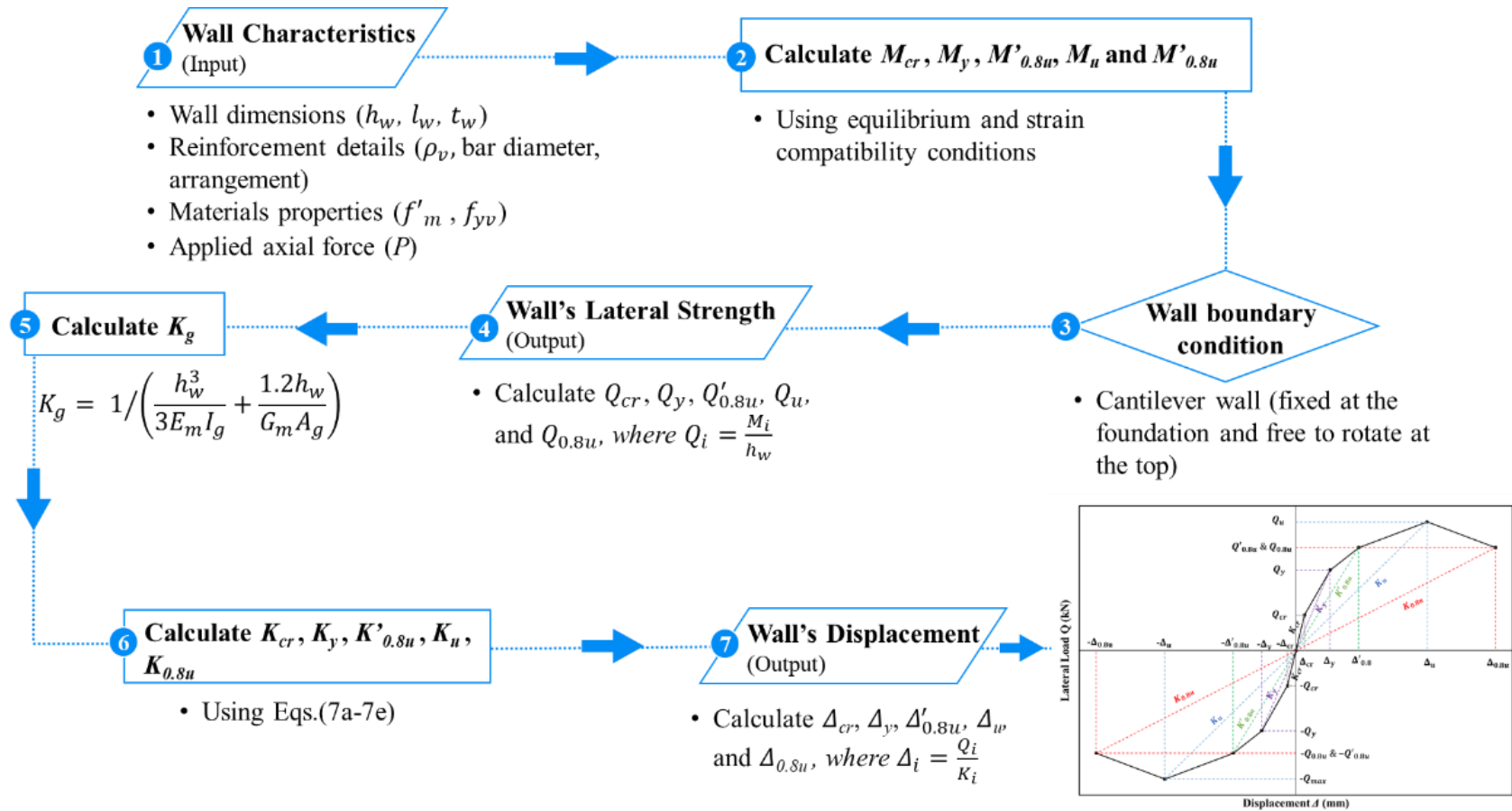


Figure 10. Procedures to generate the proposed backbone model

9. COMPONENT-LEVEL MODEL PERFORMANCE ASSESSMENT

The prediction performance of the developed MGGP-based backbone model was evaluated against that of existing backbone models that were specifically proposed for fully grouted RCBSWs. The trilinear backbone model proposed by Ashour and El-Dakhakhni [10], the quad-liner backbone model proposed by Ashour and Galal [11], and the trilinear backbone model proposed by Ezzeldin et al. [12] were used for comparison.

Figure 11 shows the comparison between the experimental backbone models of 22 RCBSWs (i.e., the testing subset) against those proposed by the MGGP model and the other existing models. As can be seen, among all the backbone models examined, the MGGP-based model showed the best ability to predict the cyclic response of RCBSWs in pre-cracking stage and up to the yielding, ultimate, and 20% strength degradation. The higher accuracy of the MGGP model compared to other existing models is attributed to (a) the relative larger dataset used in the development, which has never been utilized to develop any of the existing models, and (b) the use of robust variables selection and MGGP techniques, unlike the classic regression techniques used for developing existing models, to identify the most influential parameters and capture nonlinear relationships governing the cyclic response of RCBSWs.

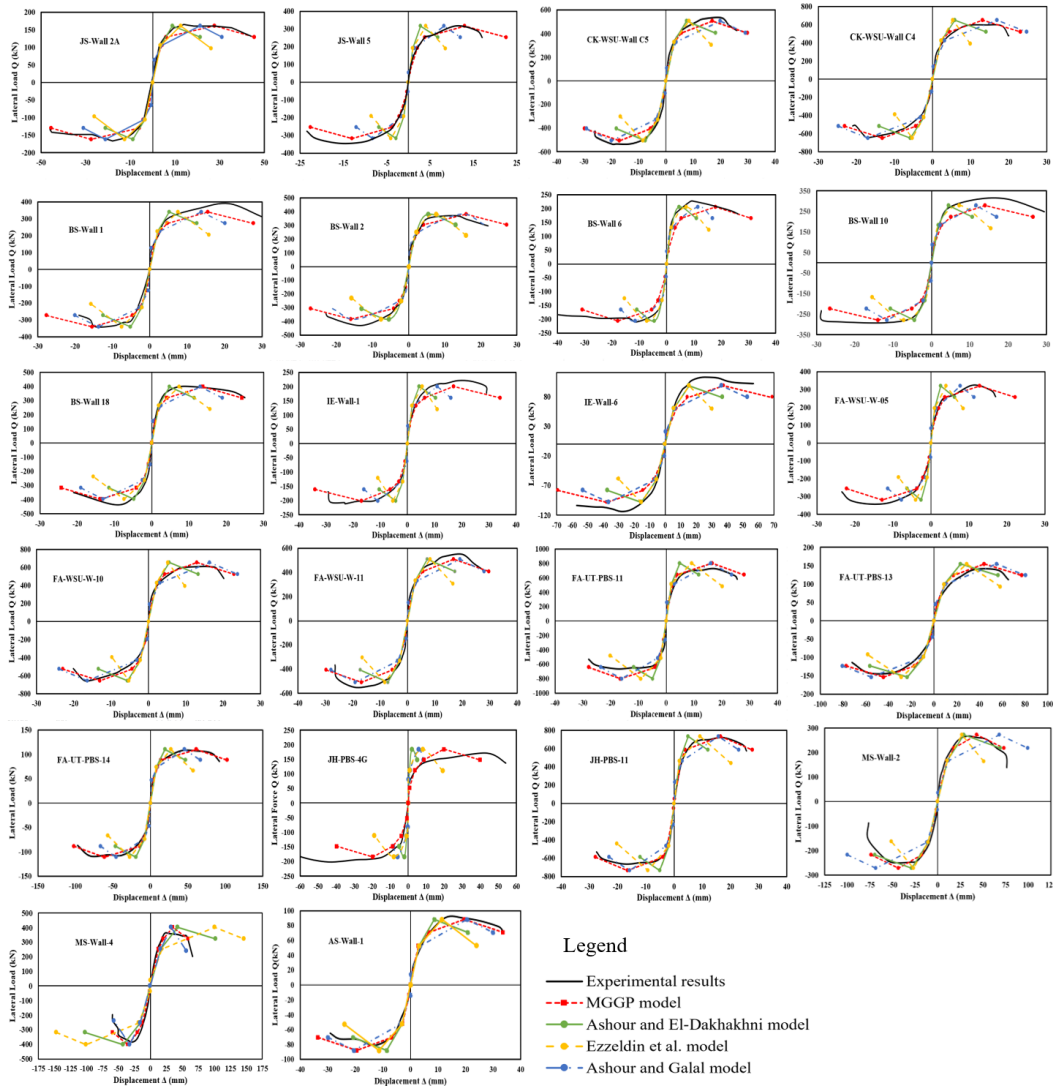


Figure 11. Predictability of the MGGP model compared to other existing models

The accuracy of the investigated models was further examined in each stage of loading. Since the strengths in all investigated models are derived using basic mechanics (i.e., force equilibrium and strain compatibility conditions), the comparison was performed based on the model capability of predicting different wall displacements. The accuracy of the predicted displacements against the experimental values was evaluated by calculating R^2 , the root of mean squared error ($RMSE$), and the mean absolute error (MAE). The mean (μ) and coefficient of variance (CV) of the experimental-to-predicted displacement ratios were also obtained to evaluate the consistency of predictions. Subsequently, the models were ranked based on the measured statistical indicators, in which the first rank (i.e., best performance) was assigned to the model having the closest μ to 1, the highest R^2 , and the lowest $RMSE$, MAE , and CV . All statistical indicators are presented in **Fig. 12**. As can be inferred from the figure, the MGGP-model ranked as the best performing model, showing the μ in a range of 1~1.06, the R^2 in a range of 0.88~0.93, and the $RMSE$, MAE , and CV in a range of 2.81~16 mm, 1.51~11.2 mm, and 26~36%, respectively. On the other hand, all other models appeared to underestimate the Δ_y , Δ_u , and $\Delta_{0.8u}$ (i.e., $\mu > 1$) with higher inconsistent predictions (i.e., higher $RMSE$, MAE , and CV). The least performing model was that proposed by Ashour and El-Dakhakhni [10] due to the very limited data used in the development, even compared to other existing models. With the increase in training dataset, the accuracy of the model improved as shown by Ashour and Galal's model—developed through updating Ashour and

El-Dakhakhni's model using larger dataset. This indicates that the size and diversity of the training dataset is a key factor in developing data-driven models. In the future, the availability of further relevant results of RCBSWs (i.e., a larger training dataset) is expected to result in improving the developed MGGP model.

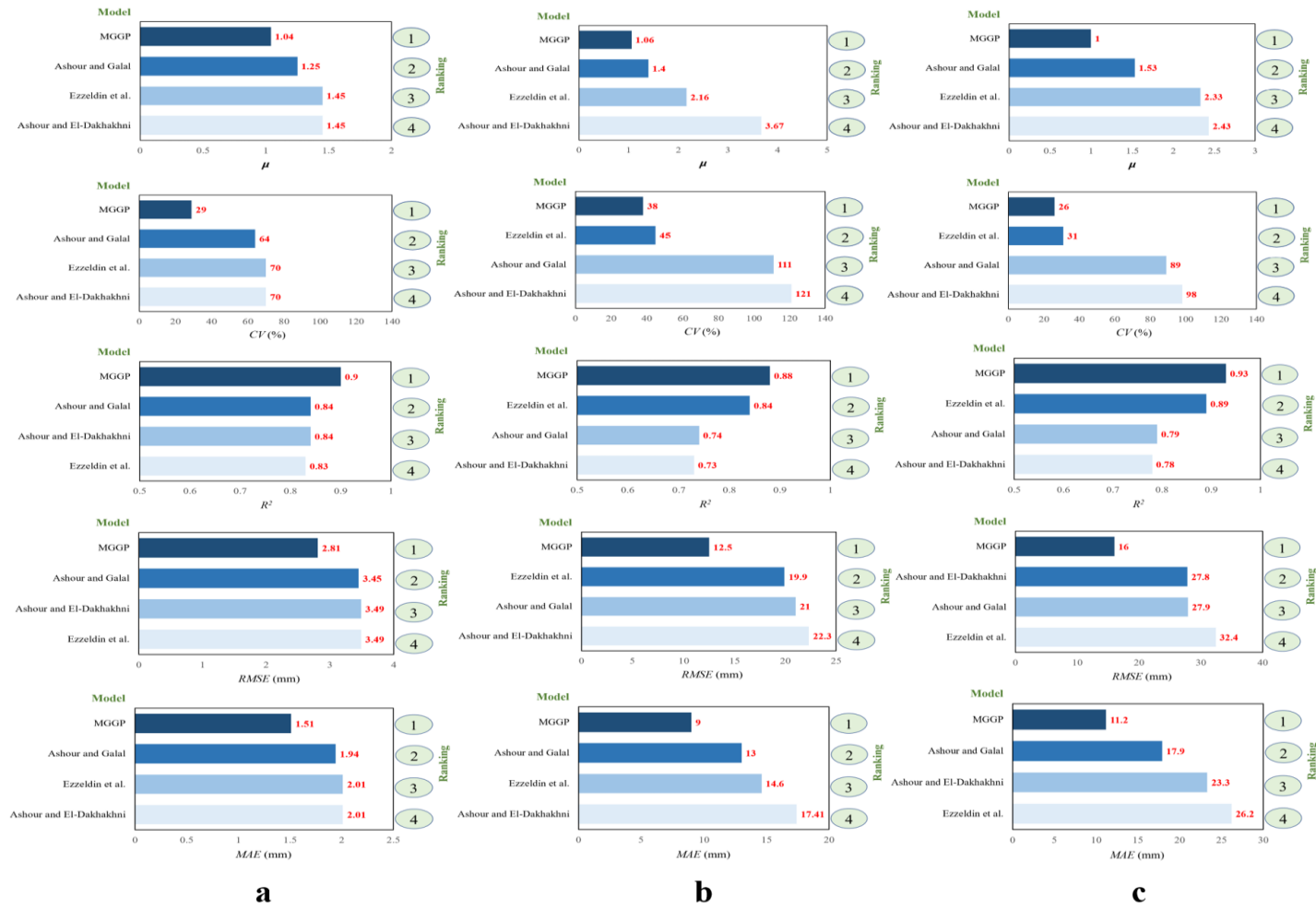


Figure 12. Statistical indicators of displacement predictions at (a) yielding, (b) ultimate, and (c) 20% strength degradation

10. SYSTEM-LEVEL MODEL PERFORMANCE ASSESSMENT

In this section, the performance of the MGGP model (proposed based on component-level experimental data) to predict the cyclic response of full RCBSW buildings (i.e., system-level) was evaluated. Two two-story RCBSW buildings constructed and tested by Heerema et al. [47-48] (Building *II*) and Ashour and El-Dakhakhni [10] (Building *III*) were used for comparison. Both buildings were identical in terms of RCBSWs' geometry, materials, reinforcement, and distribution, whereas they differed in their floor diaphragms. In Building *II*, hinge lines were introduced within the floor slab (i.e., a reduction in the floor slab thickness) to eliminate the out-of-plane diaphragm's coupling influences on the RCBSWs aligned along the loading direction. As a result, the RCBSWs in Building *II* are more likely to behave as cantilever walls. On the other hand, in Building *III*, the RCBSWs along the loading direction were restrained by the diaphragm's coupling influences induced by the floor slab and orthogonal walls. In both buildings *II* and *III*, the load was applied at the top slab level. In predicting the cyclic response of both buildings, the proposed MGGP model was used to generate the load-displacement backbone curves of all RCBSWs aligned along the loading direction (W_1 , W_2 , W_5 , and W_8), individually (as shown in **Fig. 13**), while the contribution of the walls perpendicular to the load direction were neglected due to their minimal out-of-plane stiffness. Then, the developed backbone curves were superimposed at each displacement demand level (i.e., at a

given displacement (Δ_i), the walls' strength were algebraically summed as given in Eq. 8 and presented in **Fig. 13**), to quantify the overall building response. Due to the asymmetry of the buildings' geometry, the twist measures obtained from the experiments were considered in the calculations.

$$Q_{ti} = Q_{1i} + Q_{2i} + Q_{5i} + Q_{8i} \quad (8)$$

In the MGGP model, the boundary condition of RCBSWs was simply modeled by taking the K_g similar to that stated in Eq. 2a for Building *II*, simulating the boundary condition of RCBSWs as fixed at the foundation and free to rotate at the roof level. In Building *III*, the K_g was taken similar to Eq. 9 according to Paulay and Priestley [25], assuming the boundary condition of the RCBSWs as restrained at both the foundation and the roof level. However, according to Ashour and El-Dakhakhni [10] and Ezzeldin et al. [12], in the post-peak stage, the diaphragm coupling degrades gradually as the drift level increases due to the formation of cracks within the diaphragm, until the diaphragm became incapable of preventing the RCBSWs from rotation and then they respond almost as cantilevers at large drifts. In their analysis, Ashour and El-Dakhakhni [10] assumed that beyond the ultimate load, the walls in Building *III* can be analyzed as a cantilever, neglecting the diaphragm coupling at the roof level. After reaching the ultimate load, the wall-foundation restraining levels further deteriorate, and subsequently, the assumption adopted by Ashour and El-Dakhakhni [10] (i.e., cantilever wall) may result inaccurate estimations. The analysis performed by

Ezzeldin et al. [12] assume a gradual decrease in the diaphragm's coupling accompanied with strength degradation, which was mostly eliminated at a drift level corresponding to around 40% strength reduction. By taking this analysis into consideration and assuming a linear gradual degradation in the diaphragm's coupling, the stiffness of the fifth point corresponding to the 20% strength degradation ($K_{0.8u}$) was reduced by 50%.

$$K_g = 1 / \left(\frac{h_w^3}{12E_m I_g} + \frac{1.2h_w}{G_m A_g} \right) \quad (9)$$

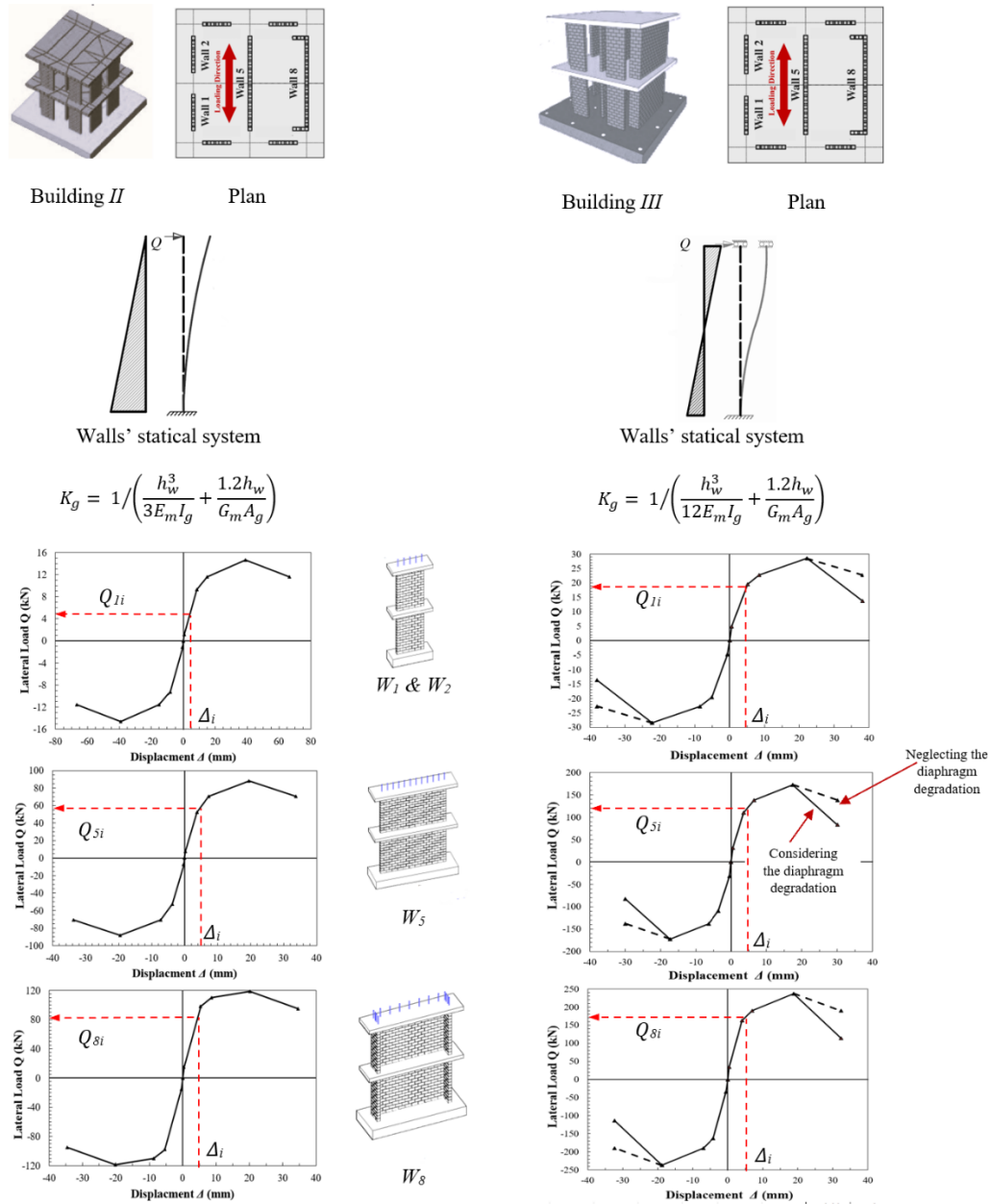


Figure 13. The predicted backbone curves of individual RCBSWs in Buildings II tested by Heerema et al. [47] and III tested by Ashour and El-Dakhkhni [10]

Figure 14 compares the predicted superimposed backbone curves with that experimentally measured for Building *II* and *III* [10, 48]. As seen, the proposed model demonstrates excellent predictability up to the yielding point. Beyond this level and up to 20% strength degradation, a slight deviation between the lateral load predictions and the experimental results was observed. This might be attributed to the significant damages that are typically induced to diaphragms and walls at such high level of loadings, which in turn affect the system-level prediction accuracy of the proposed model. However, the maximum deviations observed in Building *II* are 7.5% at yielding strength, 2% at 80 % of the ultimate strength, 10.3% at the ultimate strength, and 7% in the descending branch of the backbone curve up to reaching a 20% strength degradation (post-peak stage). These deviations are 3.4%, 6.1%, 9.4%, and 9.1%, respectively, for Building *III*. This excellent prediction accuracy, even at high levels of loading, indicates that the MGGP model proposed in this study has a promising capability to predict the cyclic response of RCBSW buildings considering the diaphragm coupling influences through the term of K_g . Subsequently, the MGGP model can be an efficient system-level prediction tool for practicing engineers and designers to help in quantifying the seismic response of RCBSW buildings. However, further validations are necessary to ensure the reliability of the proposed model for system-level predictions, especially when other wall design characteristics are considered.

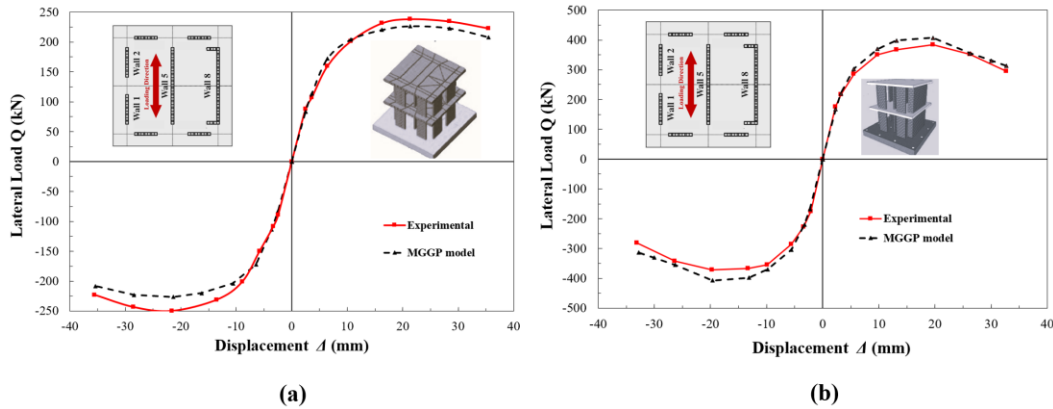


Figure 14. Superimposition of RCBSW components backbone model generated using MGGP model compared to experimental backbone model obtained from (a) Building II tested by Heerema et al. [47], and (b) Building III tested by Ashour and El-Dakhakhni [10]

11. SENSITIVITY ANALYSES

Further analysis was conducted in this study to examine the behavior of the prediction expressions to the different input parameters. **Figure 15** presents the relationship between the MGGP-based expressions (K_{cr} , K_y , $K'_{0.8u}$, K_u , $K_{0.8u}$) and the input parameters used in the modelling. These relationships were investigated by changing one parameter within its range, while the other parameters were set at their mean values. The results of the parametric analysis in **Fig. 15** show that all wall design parameters (i.e., P , l_w , t_w , f'_m , ρ_v) have direct relationships with the corresponding K_{cr} , K_y , $K'_{0.8u}$, K_u , $K_{0.8u}$ as increasing these parameters subsequently increases the stiffnesses values. On the other hand,

increasing the wall height (h_w) has a negative influence. These results agree with the basic mechanics of RCBSW systems, and therefore considered robust. To further understand the extents of the influences of each input design parameter on the developed expressions, sensitivity analysis was performed. The stiffness expressions' sensitivity to each design parameter was investigated using Eqs. 10a -10b [49]:

$$N_i = K_{MGGP \max}(x_i) - K_{MGGP \min}(x_i) \quad (10a)$$

$$S_i = \frac{N_i}{\sum_{i=1}^n N_i} \times 100 \quad (10b)$$

where, $K_{MGGP \max}(x_i)$ and $K_{MGGP \min}(x_i)$ are, respectively, the maximum and minimum stiffness predictions for each developed expression (K_{cr} , K_y , $K'_{0.8u}$, K_u , and $K_{0.8u}$), obtained from investigating the entire range of the i^{th} design parameter while all other parameters were kept constant at their mean values.

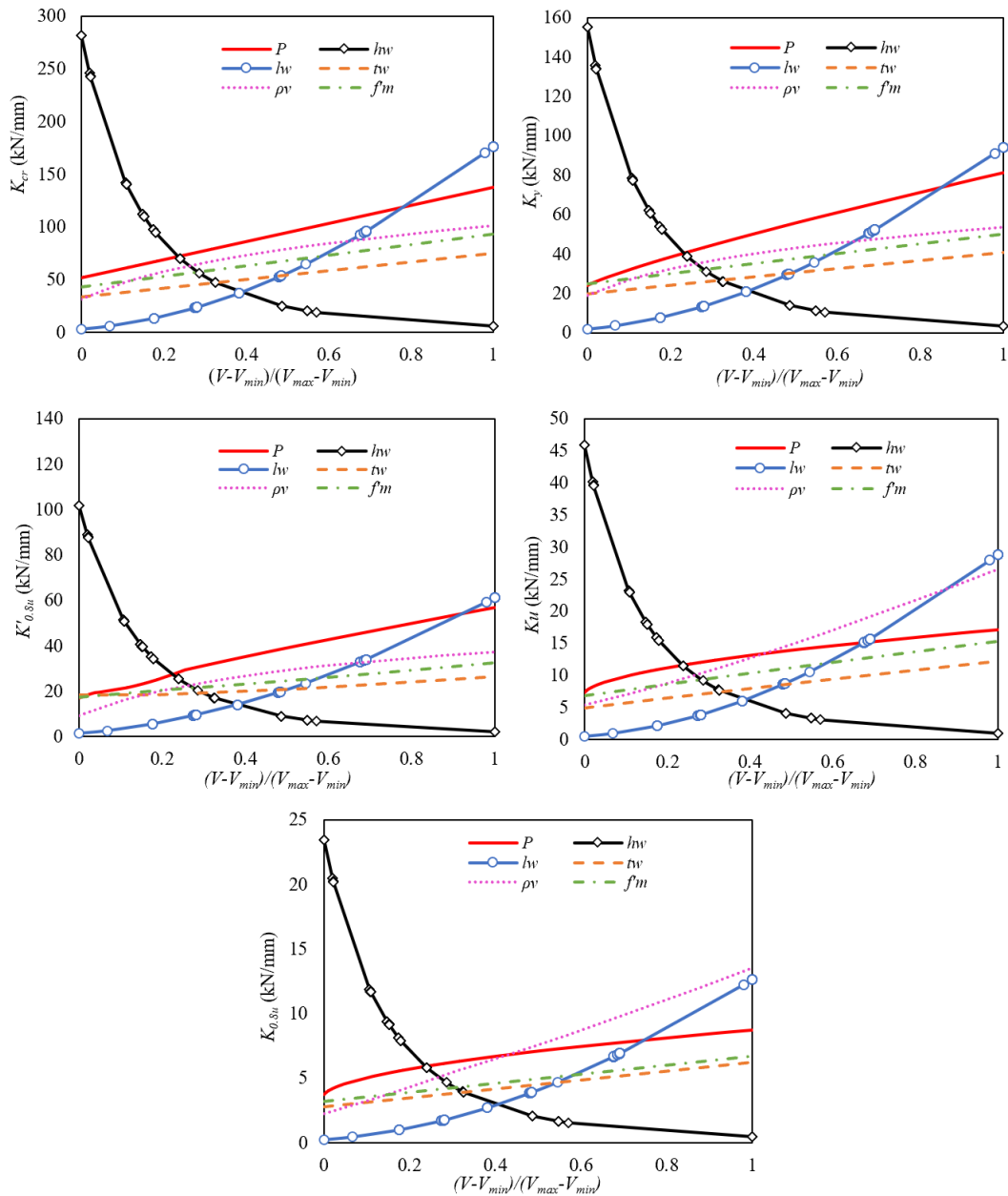


Figure 15. Effect of parameters on the performance stiffness expressions, where V refers to any independent variable from Eqs. 7a-7e

Figure 16 presents the results of the sensitivity analysis. The figure indicates that expression predictions are most sensitive to some of the walls’

geometric parameters, h_w , l_w , and P and h_w , whereas the masonry compressive strength f'_m , and the wall thickness t_w have the lowest effect on all prediction expressions. These findings conform with those reported by other researchers (e.g., Shedid et al. [30]; Ahmadi et al. [35])—further asserting robustness of the MGGP-based stiffness prediction expressions for engineering practice.

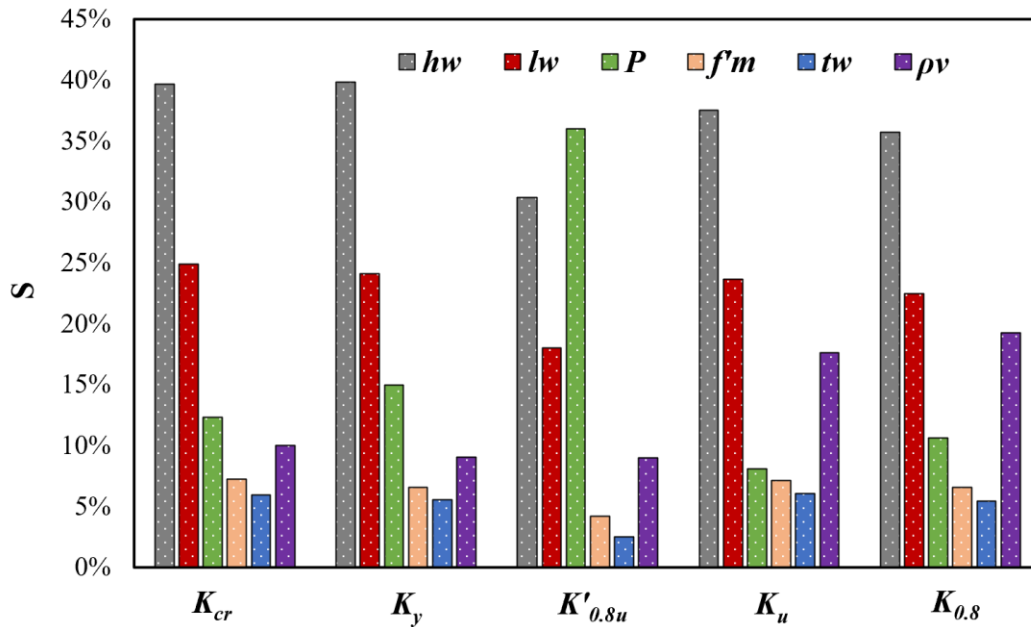


Figure 16. Sensitivity analysis of input design parameters in developed MGGP-based expressions

12. CONCLUSIONS

The current paper employed MGGP, a bio-inspired artificial intelligence technique, to efficiently develop a piecewise-linear backbone model for flexure-dominated fully grouted RCBSWs. An experimental dataset of 74 RCBSW was

collected from previous studies and utilized to train and test the MGGP expressions employed to generate the wall response backbone. A variable selection procedure was performed on the collected dataset first to identify the variables most influencing wall behavior, for each of the developed expressions. The accuracy of the MGGP-based backbone model was assessed at component- and system-level and compared to other existing models available in the literature. The main findings obtained from this study are:

- The subset selection procedure is an efficient tool for identifying the most influential input parameter and excluding the least relevant ones—avoiding unnecessary complexity in the resulting prediction expressions. The variable selection analysis showed that the axial load ratio ($P/A_w \cdot f'_m$) and the vertical reinforcement ratio (ρ_v) have a direct significant influence on the stiffness ratios, and subsequently, both variables were considered in developing the expressions.
- Compared to other existing backbone models, the developed MGGP-based model demonstrated higher accuracy in predicting the full response of RCBSWs (up to 20% strength degradation). The model can thus facilitate seismic design of new buildings and assessment of existing ones.
- The developed MGGP model was integrated with a procedure that considers the floor slab stiffness (i.e., diaphragm) influences on the cyclic response of RCBSWs at system-level, yielding a useful prediction tool for

practicing engineers and building designers.

- Further analysis showed that the expressions' stiffness predictions are positively influenced by the axial load (P), vertical reinforcement ratio (ρ_v), masonry compressive strength (f'_m), and wall thickness (t_w), whereas the increase of wall height (h_w) has an adverse influence.
- The sensitivity analysis indicated that the expressions' stiffness predictions are most sensitive to the change of wall height and length (h_w and l_w , respectively) followed by axial load (P) and vertical reinforcement ratio (ρ_v), whereas the masonry compressive strength (f'_m) and wall thickness (t_w) have the lowest effect.

In general, the study outcomes indicate promising capabilities of artificial intelligence techniques, specifically MGGP, in reasonably capturing nonlinear input-output relationships controlling complex behavior such as the cyclic behavior of RCBSWs at the component- and system-levels. This can in turn extend the application of MGGP in the interpretation of ill-defined problems in structural engineering. In closure, and similar to all data-driven models, the expressions developed here, although generalizable to other RCBSWs not used in training, they may only be valid for walls with design parameters that fall within the ranges examined. Pending the emergence of further relevant results for RCBSWs (i.e., a larger training dataset), future expression updates may be warranted.

13. REFERENCES

- [1] Pampanin, S. (2006). Controversial aspects in seismic assessment and retrofit of structures in modern times: Understanding and implementing lessons from ancient heritage. *Bulletin of the New Zealand Society for Earthquake Engineering*, 39(2), 120-133.
- [2] Astroza, M., Moroni, O., Brzev, S., & Tanner, J. (2012). Seismic performance of engineered masonry buildings in the 2010 Maule earthquake. *Earthquake Spectra*, 28(1_suppl1), 385-406.
- [3] Valdebenito, G., Alvarado, D., Sandoval, C., & Aguilar, V. (2015). Terremoto de Iquique Mw= 8, 2-01 April 2014: Observed damage and site effects on masonry structures. In *XI Chilean Congress of Seismology and Earthquake Engineering (Vol. 221)*.
- [4] Aguilar, V., Sandoval, C., Adam, J.M., Garzón-Roca, J. and Valdebenito, G. (2016). Prediction of the shear strength of reinforced masonry walls using a large experimental database and artificial neural networks. *Structure and Infrastructure Engineering*, 12(12), 1661-1674.
- [5] ASCE/SEI. ASCE standard, ASCE/SEI, 41-17 (2017). *Seismic Evaluation and Retrofit of Existing Buildings*. Reston, VA: American Society of Civil Engineers.
- [6] Canadian Standard Association. CSA S304-14, (2014). *Design of Masonry Structures*. Mississauga, Ontario, Canada.

- [7] ACI 530-05. (2011). Building Code Requirements for Masonry Structures. TMS 402-11:158.
- [8] Park, R. (1989). Evaluation of ductility of structures and structural assemblages from laboratory testing. Bulletin of the New Zealand society for earthquake engineering, 22(3), 155-166.
- [9] Thomsen IV, J. H., & Wallace, J. W. (2004). Displacement-based design of slender reinforced concrete structural walls—experimental verification. Journal of structural engineering, 130(4), 618-630.
- [10] Ashour, A., & El-Dakhakhni, W. (2016). Influence of floor diaphragm–wall coupling on the system-level seismic performance of an asymmetrical reinforced concrete block building. Journal of Structural Engineering, 142(10), 04016071.
- [11] Ashour, A., & Galal, K. (2017). Load-displacement backbone model for flexure-dominated reinforced masonry shear walls. In 13th Canadian Masonry Symposium, Halifax, Canada.
- [12] Ezzeldin, M., El-Dakhakhni, W., & Wiebe, L. (2018). Reinforced masonry building seismic response models for ASCE/SEI-41. Journal of Structural Engineering, 144(1), 04017175.
- [13] Siam, A., Ezzeldin, M., & El-Dakhakhni, W. (2019). Machine learning algorithms for structural performance classifications and predictions: Application to reinforced masonry shear walls. In Structures (Vol. 22, pp.

- 252-265). Elsevier.
- [14] Gandomi AH, Alavi AH, Arjmandi P, Aghaeifar A, Seyednour R. (2010). Genetic programming and orthogonal least squares: a hybrid approach to modeling of compressive strength of CFRPconfined concrete cylinders. *J Mech Mater Struct* 5(5):735–753
- [15] Geem, Z. W., J. H. Kim, and G. V. Loganathan. (2001). “A new heuristic optimization algorithm: Harmony search.” *Simulation* 76 (2): 60–68. <https://doi.org/10.1177/003754970107600201>.
- [16] Cladera A., J. L. Perez-Ordenez, and F. Martinez-Abella. (2014). “Shear strength of RC beams. Precision, accuracy, safety and simplicity using genetic programming.” *Comput. Concr.* 14 (4): 479–501. <https://doi.org/10.12989/cac.2014.14.4.479>.
- [17] Gandomi, A. H., Sajedi, S., Kiani, B., & Huang, Q. (2016). Genetic programming for experimental big data mining: A case study on concrete creep formulation. *Automation in Construction*, 70, 89-97.
- [18] Aval, S. B., Ketabdari, H., & Gharebaghi, S. A. (2017). Estimating shear strength of short rectangular reinforced concrete columns using nonlinear regression and gene expression programming. In *Structures* (Vol. 12, pp. 13-23). Elsevier.
- [19] Shahmansouri, A. A., Bengar, H. A., & Ghanbari, S. (2020). Compressive strength prediction of eco-efficient GGBS-based geopolymer concrete

- using GEP method. *Journal of Building Engineering*, 31, 101326.
- [20] Zhang, R., & Xue, X. (2021). A predictive model for the bond strength of near-surface-mounted FRP bonded to concrete. *Composite Structures*, 262, 113618.
- [21] Rajabi, Z., Eftekhari, M., Ghorbani, M., Ehteshamzadeh, M., & Beirami, H. (2022). Prediction of the degree of steel corrosion damage in reinforced concrete using field-based data by multi-gene genetic programming approach. *Soft Computing*, 1-16.
- [22] Gondia, A., Ezzeldin, M., & El-Dakhkhni, W. (2020). Mechanics-guided genetic programming expression for shear-strength prediction of squat reinforced concrete walls with boundary elements. *Journal of Structural Engineering*, 146(11), 04020223.
- [23] Shahnewaz, M., & Alam, M. S. (2020). Genetic algorithm for predicting shear strength of steel fiber reinforced concrete beam with parameter identification and sensitivity analysis. *Journal of Building Engineering*, 29, 101205.
- [24] M. K. Ismail, A. Yosri, and W. EL-Dakhkhni. (2022). A multi-gene genetic programming model for predicting shear strength of steel fiber concrete beams. *ACI Structural Journal*, vol. 119, No. 2, 317-328.
- [25] Paulay T, Priestley MJN. (1992). *Seismic design of reinforced concrete and masonry buildings*. New York: Wiley.

- [26] Eikanas IK. (2003). Behavior of concrete masonry shear walls with varying aspect ratio and flexural reinforcement Diss. Washington State University.
- [27] Priestley, M. J. N., & Elder, D. M. (1982). Cyclic loading tests of slender concrete masonry shear walls. *Bulletin of the New Zealand Society for Earthquake Engineering*, 15(1), 3-21.
- [28] Shing, P. B. (1991). Response of single-story reinforced masonry shear walls to in-plane lateral loads. Department of civil, environmental and architectural engineering University of Colorado.
- [29] Shedid, M. T., Drysdale, R. G., & El-Dakhakhni, W. W. (2008). Behavior of fully grouted reinforced concrete masonry shear walls failing in flexure: Experimental results. *Journal of structural engineering*, 134(11), 1754-1767.
- [30] Shedid, M. T., El-Dakhakhni, W. W., & Drysdale, R. G. (2010). Characteristics of rectangular, flanged, and end-confined reinforced concrete masonry shear walls for seismic design. *Journal of structural engineering*, 136(12), 1471-1482.
- [31] Sherman, J. D. (2011). Effects of key parameters on the performance of concrete masonry shear walls under in-plane loading (Doctoral dissertation, Washington State University).
- [32] Hernandez, J. F. (2012). Quasi-static testing of cantilever masonry shear wall segments.

- [33] Siam A, Shedid TM, Guo Y, El-Dakhakhani WW. (2015). Reliability of plastic hinge models for reinforced concrete and reinforced concrete block structural walls. In: 12th North American Masonry Conference (CD-ROM), Denver Co, USA.
- [34] Kapoi, C. M. (2012). Experimental performance of concrete masonry shear walls under in-plane loading (Doctoral dissertation, Washington State University).
- [35] Ahmadi, F., Hernandez, J., Sherman, J., Kapoi, C., Klingner, R. E., & McLean, D. I. (2014). Seismic performance of cantilever-reinforced concrete masonry shear walls. *Journal of Structural Engineering*, 140(9), 04014051
- [36] James, G., D. Witten, T. Hastie, and R. Tibshirani. (2013). Vol. 112 of *An introduction to statistical learning*, 18. New York: Springer.
- [37] Bhat, H. S., & Kumar, N. (2010). On the derivation of the bayesian information criterion. School of Natural Sciences, University of California, 99.
- [38] Prins, N. (2016). *Psychophysics: a practical introduction*. Academic Press.
- [39] Searson DP, Leahy DE, Willis MJ. (2010). GPTIPS: an open source genetic programming toolbox for multigene symbolic regression. Proceedings of international multi conference on engineering computer science, Hong Kong

- [40] Ahangar-Asr, A., Faramarzi, A., Mottaghifard, N., & Javadi, A. A. (2011). Modeling of permeability and compaction characteristics of soils using evolutionary polynomial regression. *Computers & Geosciences*, 37(11), 1860-1869.
- [41] Koza JR. (1992). *Genetic programming, on the programming of computers by means of natural selection*. MIT Press, Cambridge
- [42] Gandomi, A. H., & Alavi, A. H. (2012). A new multi-gene genetic programming approach to nonlinear system modeling. Part I: materials and structural engineering problems. *Neural Computing and Applications*, 21(1), 171-187.
- [43] Koza, J. R. (1994). *Genetic programming II: automatic discovery of reusable programs*. MIT press.
- [44] Gandomi AH, Alavi AH, Arjmandi P, Aghaeifar A, Seyednour R. (2010). Genetic programming and orthogonal least squares: a hybrid approach to modeling of compressive strength of CFRPconfined concrete cylinders. *J Mech Mater Struct* 5(5):735–753
- [45] Cladera A., J. L. Perez-Ordóñez, and F. Martínez-Abella. (2014). “Shear strength of RC beams. Precision, accuracy, safety and simplicity using genetic programming.” *Comput. Concr.* 14 (4): 479–501. <https://doi.org/10.12989/cac.2014.14.4.479>.
- [46] Gandomi, A. H., D. Mohammadzadeh, J. L. Pérez-Ordóñez, and A. H.

- Alavi. (2014b). “Linear genetic programming for shear strength prediction of reinforced concrete beams without stirrups.” *Appl. Soft Comput.* 19 (Jun): 112–120. <https://doi.org/10.1016/j.asoc.2014.02.007>.
- [47] Heerema, P., Shedid, M., & El-Dakhakhni, W. (2015). Seismic response analysis of a reinforced concrete block shear wall asymmetric building. *Journal of structural engineering*, 141(7), 04014178.
- [48] Heerema, P., Shedid, M., Konstantinidis, D., & El-Dakhakhni, W. (2015). System-level seismic performance assessment of an asymmetrical reinforced concrete block shear wall building. *Journal of Structural Engineering*, 141(12), 04015047.
- [49] Gandomi, A. H., G. J. Yun, and A. H. Alavi. (2013). “An evolutionary approach for modeling of shear strength of RC deep beams.” *Mater. Struct.* 46 (12): 2109–2119. <https://doi.org/10.1617/s11527-013-0039-z>.